Quantifying non-Gaussian intermittent fluctuations in physiology: Multiscale probability density function analysis using the Savitzky-Golay detrending

Madhur Mangalam [*]

Department of Biomechanics and Center for Research in Human Movement Variability, Division of Biomechanics and Research Development, University of Nebraska Omaha, Omaha, Nebraska 68182, USA

Damian G. Kelty-Stephen

State University of New York at New Paltz, New Paltz, New York 12561, USA

Junichiro Hayano

Graduate School of Medicine, Nagoya City University, Nagoya, Aichi 467-8601, Japan

Eiichi Watanabe

Division of Cardiology, Department of Internal Medicine, Fujita Health University Bantane Hospital, Nagoya, Aichi 454-0012, Japan

Ken Kiyono [†]

Graduate School of Engineering Science, Osaka University, Osaka 560-8531, Japan

When measuring physiological data, the central limit theorem typically implies a consistent variance, resulting in data that closely follow a Gaussian distribution. However, physiological measurements often deviate from this expectation, increasing variance due to nonlinear correlations across various scales. The challenge lies in testing these tails, which comprise only rare and extreme values. We introduce multiscale probability density function (PDF) analysis, a method that estimates this non-Gaussianity parameter for physiological fluctuations in each of multiple timescales. We gain valuable insights into the observed distributions with heavier tails and nonlinear correlations by exploring the relationship between non-Gaussianity and logarithmic scale. To maintain the fidelity of the original data, we incorporate an adaptive detrending filter into our multiscale PDF analysis. This filter effectively eliminates trends without distorting the distribution in a way that might risk artifactual signatures of non-Gaussianity. Additionally, we explain why multiscale PDF analysis is especially well suited for examining data that follow lognormal distributions. In the final stretch, we demonstrate how multiscale PDF analysis can provide fresh perspectives on heart rate variability and postural control. This innovative approach can facilitate diagnoses in health and disease while also deepening our comprehension of how constraints influence human physiological performance.

I. INTRODUCTION

Adaptive behavior means meeting task demands without becoming rigidly locked in. It involves balancing short-term and long-term demands, requiring switching between tasks and constraints [1–3]. For example, we may interrupt writing to answer a phone call and return to writing afterward. This flexibility is observed in humans and in bacteria, cells, and parasites [4–10], foraging wild animals [11–13], human hunter-gatherers [14,15], economic markets [16–18], human behavioral organization [19–23], and various other complex systems [24–26].

The capacity of adaptive behavior to switch irregularly between multiple modes is a form of *intermittency* (or heterogeneity of variance)—a mathematical way to describe subtle irregularities that characterize the free-ranging aspect of adaptive behavior [27,28]. In the realm of dynamical systems, particularly in the context of turbulent flows, the Pomeau-Manneville scenario emerges as a prominent concept, elucidating the journey towards chaos, often referred to as turbulence, triggered by intermittency [29,30]. One of the widely explored manifestations of intermittency is the on-off intermittency, characterized by a nonperiodic oscillation between static or laminar behavior and abrupt, chaotic bursts of oscillation: random alternation between phases with extremely low movement amplitudes and phases with high movement amplitudes [31,32]. In simpler terms, *intermittency*

---

*Corresponding author: mmangalam@unomaha.edu
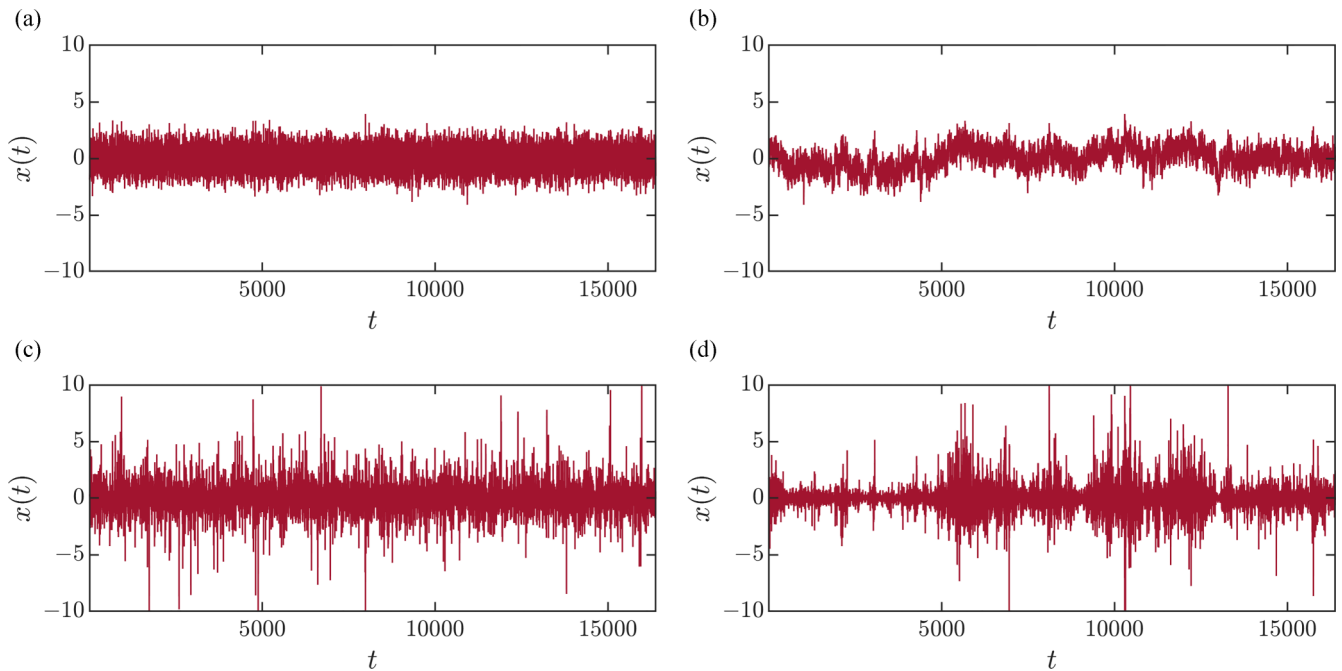†Corresponding author: kiyono.ken.es@osaka-u.ac.jp

FIG. 1. Intermittent non-Gaussian fluctuations. (a) Independent and identically distributed Gaussian fluctuations. (b) Gaussian intermittent fluctuations with long-range correlated variance. (c) Independent and identically distributed non-Gaussian fluctuations. (d) Non-Gaussian intermittent fluctuations. In this process, the variance shows long-range correlations.

means the variance in heterogeneity across time, as shown in Fig. 1(d). For instance, intermittency in heart rate variability reflects cardiac sympathetic activity due to external contexts [33,34]. Posture is similarly intermittent; postural dexterity entails swaying to support optic flow and eye and head movement [35,36]. Beyond satisfying local constraints of maintaining a stable stance, while the body sways to explore the surroundings, excessive sway topples the body, and insufficient sway leaves it poorly poised for ongoing events [37–39]. In these instances, the key characteristic of intermittency is its ability to produce a considerable number of extreme responses while maintaining an integral, coherent process. This cascadelike pattern allows for adaptation to ongoing changes in constraints on function, even though the responses may fall within the average range of other responses.

Modeling intermittency is challenging since the ability to switch between different modes of activity may seem incompatible with the rule-following of an "internal" predictive model [40–46]. The goal of modeling is to create independent symbols that can be computationally described [47]. However, context-sensitive intermittency may result from multiple causal factors that are not independent, but interact. Therefore modeling intermittency in physiology requires independent symbols representing the inadequacy of summed independent causal factors rather than encoding the measurement series through a set of independent symbols representing independent causal factors. A lengthy and relentless debate exists on how to model measurements to test whether fluid, intermittent processes depend on strongly nonlinear interactions and not independent factors [48,49]. The Gaussian probability density functions (PDFs)—the summed consequence of many independent random factors—have been a reliable workhorse

for modeling intermittency in physiology composed of independent factors [50]. However, the failure of Gaussianity or independence has been linked to adaptive context-sensitive behavior, and a different class of modeling is needed to organize the mounting quantitative evidence of this relationship [51,52].

II. NON-GAUSSIANITY AS A MEASURE OF INTERMITTENCY

Adaptive behavior involves frequent variations, allowing for exploration of more extreme regions of the state space beyond the average goal position, as described by Kelso and co-workers [53,54]. As a result, intermittent behaviors do not conform to a Gaussian distribution with short tails but instead exhibit long and heavy tails. PDFs can assess the degree to which a phenomenon is locked into the average position versus how fluidly it moves between local tasks and exploration beyond local constraints. The smoothness of the peak-to-tail transition in the PDF reveals the extent to which the phenomenon is non-Gaussian.

Gaussian distributions result from adding many independent variables, but interactions between variables in cascades promote intermittent uneven growth of variance with timescale. Multiplicative processes such as cascades produce lognormal distributions, which differ from normal distributions in that the product of independent factors generates the former. This leads to longer, heavier tails than Gaussian distributions due to nonlinear correlations [55,56]. However, testing these tails can be challenging, as rare, extreme values sparsely populate them and may be influenced by measurement artifacts, nonstationarity, or other sources of non-Gaussianity (Fig. 1) [57–60]. Fortunately, an analytical

method for estimating non-Gaussianity has emerged from research on hydrodynamic turbulence. This method involves querying distribution regions that are better populated at multiple timescales [61,62].

Multiscale PDF analysis allows us to elaborate this marginal difference in variance into a powerful tool for numerical estimation of non-Gaussianity. The theory and research on hydrodynamic cascades suggest that we can, in empirical measurements, find signatures of cascade dynamics through the change of this marginal difference between lognormal and normal variance across multiple timescales. Multiscale PDF analysis addresses the change of non-Gaussianity across scales to control for spurious effects, for example, effects of multiple-sized events due to nonstationarity.

III. MULTISCALE PDF ANALYSIS TO QUANTIFY NON-GAUSSIAN INTERMITTENT FLUCTUATIONS IN PHYSIOLOGY

This tutorial aims to introduce multiscale PDF analysis to quantify and explain intermittent fluctuations in physiology. Multiscale PDF analysis has proven helpful beyond fluid dynamics, with applications in discerning the endogenous dynamics underlying cardiac physiology [33,34,63–65] (see also Refs. [66–68]) and human postural control [69–72]. For example, non-Gaussianity in heart rate variability has been linked to increased sympathetic activity [73,74]. In contrast, non-Gaussianity in postural sway has been found to exhibit distinct signatures of both endogenous and exogenous postural demands [69–72]. Multiscale PDF analysis can help distinguish the specific contributions of various constraints to the interactivity that intermittency entails. By modeling non-Gaussianity at multiple scales, our models can precisely grasp cascadelike interactivity, allowing us to explain intermittent physiological fluctuations.

This work showcases the multiscale PDF analysis by outlining the optimal approaches for estimating non-Gaussianity across various scales, accounting for event-size heterogeneity and nonstationarity, common issues in standard investigations. We also provide an in-depth description of surrogate testing that verifies whether observed non-Gaussianity reflects nonlinear temporal correlations. To illustrate the methodology, we offer several simulations and empirical physiological time series.

IV. THE ESTIMATOR OF NON-GAUSSIANITY, λ^2

Intermittent fluctuations with heterogeneity in variance can be modeled by assuming a doubly stochastic process $x(t)$ described by

$$x(t) = \xi(t)e^{\omega(t)}, \tag{1}$$

where $\xi(t)$ is a Gaussian random variable with zero mean and $\omega(t)$ is the other Gaussian random variable independent of $\xi(t)$. $e^{\omega(t)}$ in Eq. (1) describes the fluctuation of local standard deviations, which results in the non-Gaussian distribution of $x(t)$.

This framework forms the basis of Castaing's PDF model, introduced as a model of the velocity difference between two points in fully developed turbulent flows [61]. In addition, this framework also encompasses the Beck-Cohen superstatistical distributions introduced as a model of complex nonequilibrium systems [75,76]. The standardized PDF of $x(t)$ is given by

$$f_\lambda(x) = \int_0^\infty \frac{1}{\sqrt{2\pi}\lambda} \exp\left(-\frac{(\ln\sigma + \lambda^2)^2}{2\lambda^2}\right)$$
$$\times \frac{1}{\sqrt{2\pi}\sigma} \exp\left(-\frac{x^2}{2\sigma^2}\right) d(\ln\sigma), \tag{2}$$

where λ^2 is the non-Gaussian parameter. $\lambda^2 \to 0$ in Eq. (2) yields a Gaussian distribution. In contrast, the larger values of λ^2 yield fatter non-Gaussian tails of the PDF (Fig. 2).

The time series' non-Gaussian parameter, λ^2 (assuming unit variance, i.e., $\sigma = 1$), can be estimated using a moment-based estimator

$$\hat{\lambda}_q^2 = \frac{2}{q(q-2)}\left\{\ln\left(\frac{\sqrt{\pi}\langle|x|^q\rangle}{2^{q/2}}\right) - \ln\Gamma\left(\frac{q+1}{2}\right)\right\} \quad (q \neq 0, 2)$$

$$\hat{\lambda}_0^2 = \lim_{q\to 0}\lambda_q^2 = -\langle\ln|x|\rangle - \frac{\gamma + \ln 2}{2} \quad (q = 0)$$

$$\hat{\lambda}_2^2 = \lim_{q\to 2}\lambda_q^2 = -\langle x^2\ln|x|\rangle - \frac{\gamma + \ln 2}{2} - 1 \quad (q = 2), \tag{3}$$

where $\hat{\lambda}_q^2$ is the estimated value of the non-Gaussian parameter for the qth absolute moment, λ^2, angular brackets mean the statistical average, Γ is the gamma function, and the moment $q > -1$.

The other non-Gaussian parameter corresponding to the variance of $\omega(t)$ in Eq. (1) is given by the log-amplitude-based estimator

$$\hat{\lambda}^2 = \langle(\ln|x| - \langle\ln|x|\rangle)^2\rangle - \frac{\pi^2}{8}; \tag{4}$$

the details have been provided in previous work [75,76].

A. Relationship between the estimator of non-Gaussianity, λ^2, and kurtosis, a canonical measure of non-Gaussianity in glassy systems

A canonical measure of non-Gaussianity in glassy systems is kurtosis, $K = \frac{\langle x^4\rangle}{\sigma^4}$ [77,78]. The quantity K is a key indicator for assessing the extent to which the distribution of $x(t)$ deviates from the Gaussian distribution. $K > 0$ signifies an expansion in the $x(t)$ distribution, implying that significant events are more heavily weighted than the Gaussian distribution. It is essential to note that kurtosis provides little insight
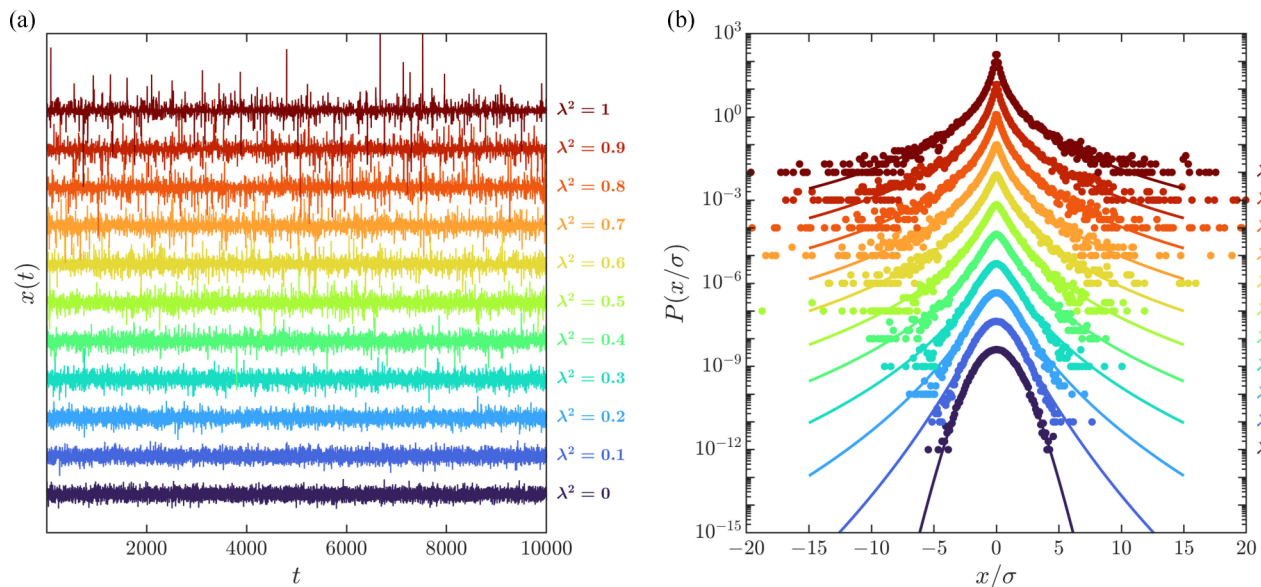
(a)

(b)

FIG. 2. Non-Gaussian intermittent fluctuations. (a) Simulated time series with varying degrees of non-Gaussianity, represented by the parameter λ^2 defined by Eq. (1). (b) The corresponding theoretical and empirical PDFs are plotted in linear-log coordinates. As λ^2 increases, the PDF becomes more sharply peaked and has heavier tails. Conversely, as λ^2 decreases, the PDF resembles a Gaussian distribution, approaching a perfect Gaussian distribution as λ^2 approaches zero. The solid lines on the graph represent the numerical integration of Eq. (2), while the symbols show the estimated PDFs obtained from the time series in (a). The PDFs have been vertically shifted for ease of presentation, and the vertical axis is given in arbitrary units.

into the precise shape of the peak; its unambiguous interpretation lies in its ability to describe the extremity of tails. This interpretation relates to the presence of outliers, in the case of sample kurtosis, or the likelihood of generating outliers, as seen in the kurtosis of a probability distribution.

The kurtosis is equivalent to our moment-based estimator in Eq. (3) with $q = 4$. Substituting $\frac{x}{\sigma}$ for x in Eq. (3), given that Eq. (3) assumed unit variance, we get

$$\hat{\lambda}_q^2 = \frac{2}{q(q-2)} \left\{ \ln \left(\frac{\sqrt{\pi} \langle |\frac{x}{\sigma}|^q \rangle}{2^{q/2}} \right) - \ln \Gamma \left(\frac{q+1}{2} \right) \right\}.$$

When $q = 4$,

$$\hat{\lambda}_4^2 = \frac{1}{4} \left\{ \ln \left(\frac{\sqrt{\pi} \langle |\frac{x}{\sigma}|^4 \rangle}{4} \right) - \ln \Gamma \left(\frac{5}{2} \right) \right\}$$

$$= \frac{1}{4} \left\{ \ln \left(\frac{\sqrt{\pi} \langle |\frac{x}{\sigma}|^4 \rangle}{4} \right) - \ln \frac{3\sqrt{\pi}}{4} \right\}$$

$$= \frac{1}{4} \ln \frac{\frac{\sqrt{\pi}}{4} \langle |\frac{x}{\sigma}|^4 \rangle}{\frac{3\sqrt{\pi}}{4}}$$

$$= \frac{1}{4} \ln \frac{1}{3} \frac{\langle x^4 \rangle}{\sigma^4}$$

$$= \ln \frac{1}{3} K;$$

that is,

$$\frac{1}{3} K = e^{\hat{\lambda}_4^2}. \tag{5}$$

To compare the accuracy of the moment-based non-Gaussian parameter [Eq. (3)] and kurtosis [Eq. (5)], we generated independent and identically distributed non-Gaussian time series

with different theoretical values of λ^2 using the standardization of Eq. (1), as in Fig. 2:

$$x(t) = \xi(t) e^{\lambda \omega(t) - \lambda^2}, \tag{6}$$

where $\xi(t)$ is a Gaussian random variable with zero mean and unit variance and $\omega(t)$ is the other Gaussian random variable with zero mean independent of $\xi(t)$. Figure 3 shows the estimated values of $\hat{\lambda}_q^2$ averaged over 1024 iterations. If the time series is sufficiently long [$n \approx 10^6$ and $n \approx 10^5$ in Figs. 3(a) and 3(b), respectively], $\hat{\lambda}_q^2$ provides a consistent estimation of non-Gaussianity until higher order q. $\hat{\lambda}_q^2$ for $0 < q < 1$ still provides a consistent estimation of non-Gaussianity when the time series length $n \approx 10^4$ [Fig. 3(c)]. Only for time series with $n \approx 10^3$ does $\hat{\lambda}_q^2$ show both considerable variability and dependence on q [Fig. 3(d)]. However, when $q = 4$, $\hat{\lambda}^2$ is extremely sensitive to the PDF tails. In other words, when $q = 4$, $\hat{\lambda}^2$ is mainly determined by a small number of extreme outliers. Thus the kurtosis-based estimation accuracy of non-Gaussianity is low compared with that of $\hat{\lambda}^2$ for smaller q moments.

B. Contribution of the observed values in the estimation of the non-Gaussian parameter $\hat{\lambda}^2$

The multiscale PDF analysis is a robust approach for investigating cascadelike intermittency due to its ability to capture the broader midsection of the PDF effectively. In contrast, the maximum likelihood estimation (MLE) modeling approach primarily focuses on the tails of the distribution. While MLE is commonly employed for identifying non-Gaussianity, it tends to be sensitive to outliers and can mistakenly identify light-tailed distributions as heavy-tailed ones [58], such as
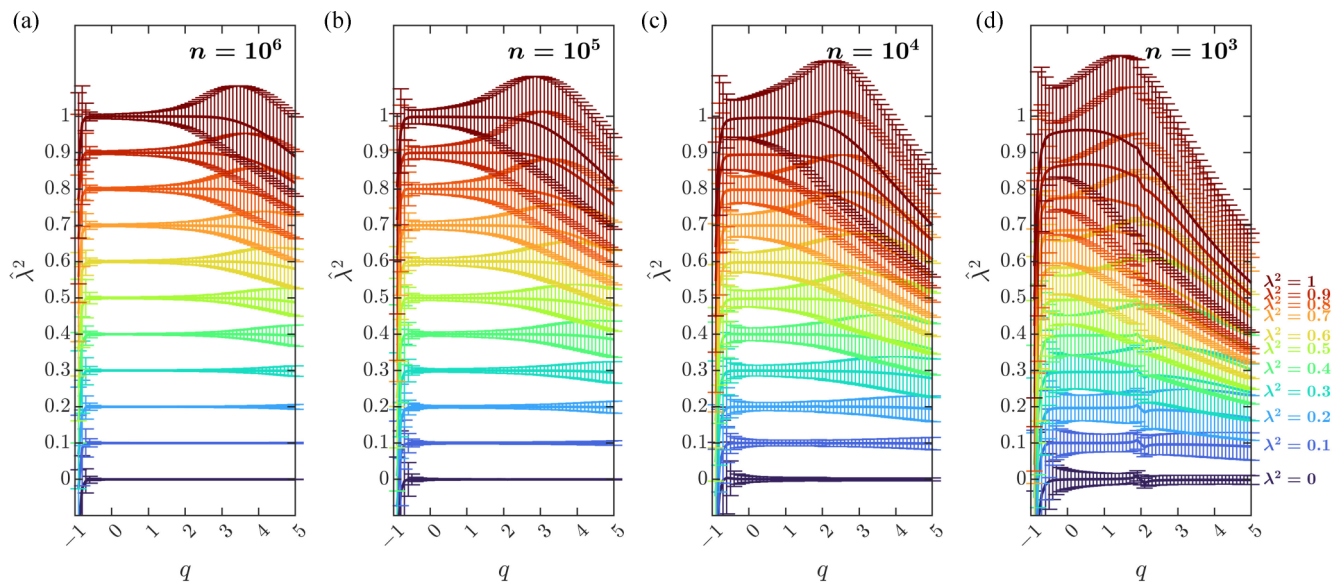
FIG. 3. Sample mean of moment-based estimator of non-Gaussianity, $\hat{\lambda}_q^2$, for different theoretical values of λ^2. The sample mean is numerically obtained across 1024 iterations. Values given in the key on the right indicate the theoretical values of $\hat{\lambda}_q^2$. The error bars indicate the sample standard deviation. (a) Time series' length $n = 10^6$, (b) $n = 10^5$, (c) $n = 10^4$, and (d) $n = 10^3$.

the lognormal distribution [79–81]. In contrast, the multiscale PDF analysis prioritizes the midsection of the PDF and examines whether its bell-like shape aligns with non-Gaussian distributions. This method employs the qth-order absolute moment, where higher and lower values of q correspond to smaller and larger fluctuations. A low value of q spreads out the midsection of the bell-shaped curve while compressing the tails. Using q effectively accentuates the well-populated midsection, offering a diagnostic tool to identify non-Gaussianity without relying on heavy tails.

The weighting assigned to the estimator $\hat{\lambda}^2$ relies on both the absolute moment and the position of the non-Gaussian distribution. When the moment order is close to zero or negative, the emphasis is placed on the central portion of the distribution. Conversely, higher orders of moment allocate greater significance to the distribution's tails. To assess these weights in the moment-based estimation of λ^2, we computed the contributions of the non-Gaussian distribution to the estimated values of λ^2 using the following expression:

$$w(x)\,dx = \frac{M(x)\,f(x)\,dx}{\int_{-\infty}^{\infty} M(x)\,f(x)\,dx}, \qquad (7)$$

where $M(x)$ is the moment estimator and $f(x)$ is the PDF of x. The relative contribution of various sections of the PDF depends less on q for smaller values of λ^2 compared with larger values [e.g., see Figs. 4(a) and 4(d); see also Figs. 4(b) and 4(c)]. In the case of large λ^2, the bulkier midsection of the PDF plays the most significant role in the moment-based estimation of λ^2 for small positive values of q, particularly notable for $q = 0.25$. However, as q increases, the estimation gradually becomes more influenced by outliers. Similar patterns are observed in the log-amplitude-based estimation of λ^2, with the bulkier midsection of the PDF having a disproportionate contribution. This trend persists even for negative values of q (e.g., $q = -0.25$), but in such cases, the

estimation completely disregards outliers while overemphasizing the contribution of the bulkier midsection.

The qth-order absolute moment helps address the longstanding challenge of estimating non-Gaussianity. By emphasizing fluctuations of different sizes, it allows for assessing the presence of distinct non-Gaussianity regimes within the same time series. While the multiscale PDF analysis already captures a significant portion of the heterogeneity in cascade-like intermittency by examining multiple timescales, it has its limitations. The assumption that small events occur over short timescales and large events occur over long timescales is not always accurate. Intermittency can lead to abrupt and frequent large events within short timescales, while longer timescales remain relatively quiet. q offers a complementary perspective on the heterogeneity of fluctuations present in non-Gaussianity. This broader approach allows for a more comprehensive understanding of the diverse manifestations of non-Gaussian behavior within the time series.

C. Random cascade process

We used a simple cascade model called the random cascade process generated using the multiplicative lognormal model to test the proposal of the multiscale PDF analysis. The numerical procedure to generate a sample time series is as follows: First, a time series $\{\xi(t)\}_{t=1}^{2^m}$ of a Gaussian noise with zero mean and variance σ_0^2 is generated, where m is the number of cascade steps. In the first cascade step ($j = 1$), the whole interval is divided into two equal subintervals and $\xi(t)$ in each subinterval is multiplied by random weights $\exp[\omega^{(1)}(k)]$ ($k = 0, 1$), where $Y^{(j)}$ are identically distributed independent random values. In the framework of Kolmogorov's refined similarity hypothesis, the PDF of $\omega^{(j)}$ is assumed to be an infinitely divisible distribution $G_0(\omega)$. In the next cascade step ($j = 2$), each subinterval is further divided into two equal subintervals, which is followed by the application of random
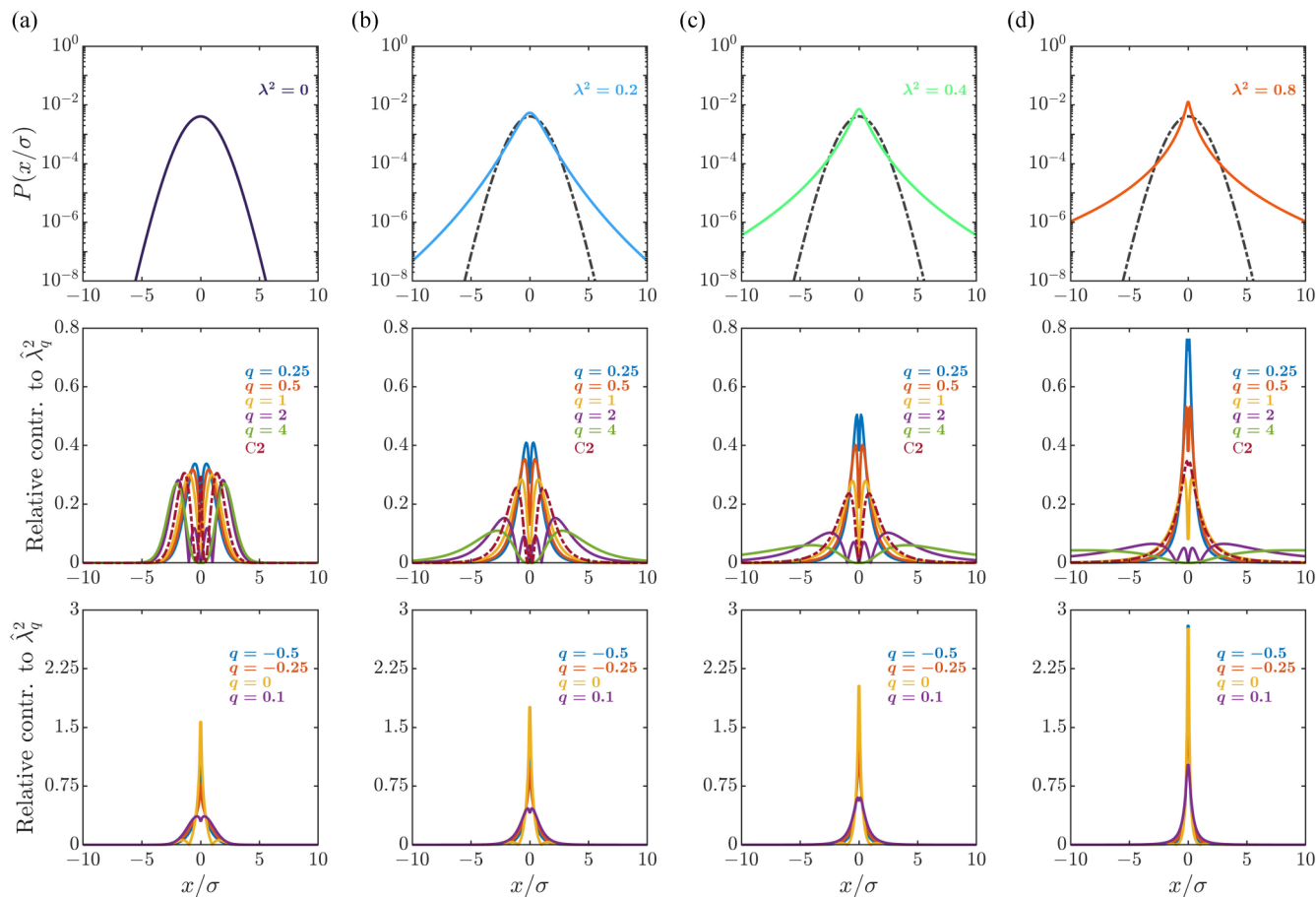
FIG. 4. Relative contributions of different parts of the PDF to the log-amplitude- and moment-based estimations of the non-Gaussian parameter, $\hat{\lambda}^2$ and $\hat{\lambda}_q^2$, for (a) $\lambda^2 = 0$, (b) $\lambda^2 = 0.2$, (c) $\lambda^2 = 0.4$, and (d) $\lambda^2 = 0.8$. The dashed line denotes a Gaussian distribution for comparison. Relative contr., relative contribution.

weights $\exp[\omega^{(2)}(k)]$ ($k = 0, 1, 2$). The same procedure is repeated, and after m steps, the time series $x(t)$ is

$$x(t) = \xi(t) \exp \sum_{j=1}^{m} \omega^{(j)}\left(\left\lfloor \frac{t-1}{2^{m-j}} \right\rfloor\right), \qquad (8)$$

where $\lfloor \cdot \rfloor$ is the floor function. If the PDF of $\omega^{(j)}$ is an infinitely divisible distribution $G_0(\omega)$, the time series $x(t)$ is described by the multiplicative lognormal model as $x(t) = \xi(t) \exp \overline{\omega(t)}^{(m)}$, where $\overline{\omega(t)}^{(m)} = \sum_{j=1}^{m} \omega^{(j)}$ and its PDF is given by m-fold convolutions of $G_0(\omega)$. Moreover, if we approximate the distribution of the local sum of $x(t)$ by a Gaussian, the local sum $\Delta_{s_n} y$ at scale $s_n = 2^{m-n}$ is approximately given by $\Delta_{s_n} y = \overline{\xi}^{s_n} \exp \overline{\omega}^{s_n}$, where $\overline{\xi}^{s_n} = \sum_{k=1}^{s_n} \xi_k$ and $\overline{\omega}^{s_n} = \sum_{j=1}^{n} \omega^{(j)}$. In this model, the non-Gaussian parameter $\hat{\lambda}^2$ of $\Delta_{s_n} y$ is estimated as

$$\lambda^2 \approx \mu_2^{(0)}(N - \log_2 s_n) \sim -\ln s, \qquad (9)$$

where $\mu_2^{(0)}$ is the variance of $\omega^{(j)}$ and s is the scale (length) of the local sum.

D. The Savitzky-Golay detrending filter

Multiscale PDF analysis involves detrending the nonstationary trends present in time series. This detrending process is crucial for maintaining the reproductive property of the normal distribution while preventing any distortion in the estimated PDF. However, the detrending procedures employed in detrended fluctuation analysis [82–85] and previous multiscale PDF analyses, such as piecewise-regression-based methods [34,63,64,69–74], utilize nonlinear filters. These filters lack the reproductive property of normal distribution. Consequently, when employing these nonlinear filters in multiscale PDF analysis, the accurate characterization of the normal distribution is compromised.

To overcome these challenges, we have adopted the Savitzky-Golay detrending filter [86,87], which ensures that the time series retains the reproductive property of the normal distribution during the detrending process. The Savitzky-Golay filter is an advanced version of the simple moving-average filter. It computes the filtered time series by evaluating the value of the least-squares polynomial at the central point within each subinterval, utilizing a window length of s. The Savitzky-Golay filter relies on two parameters: the order of the least-squares polynomial, m, and the length of the subinterval, s. Notably, m must be
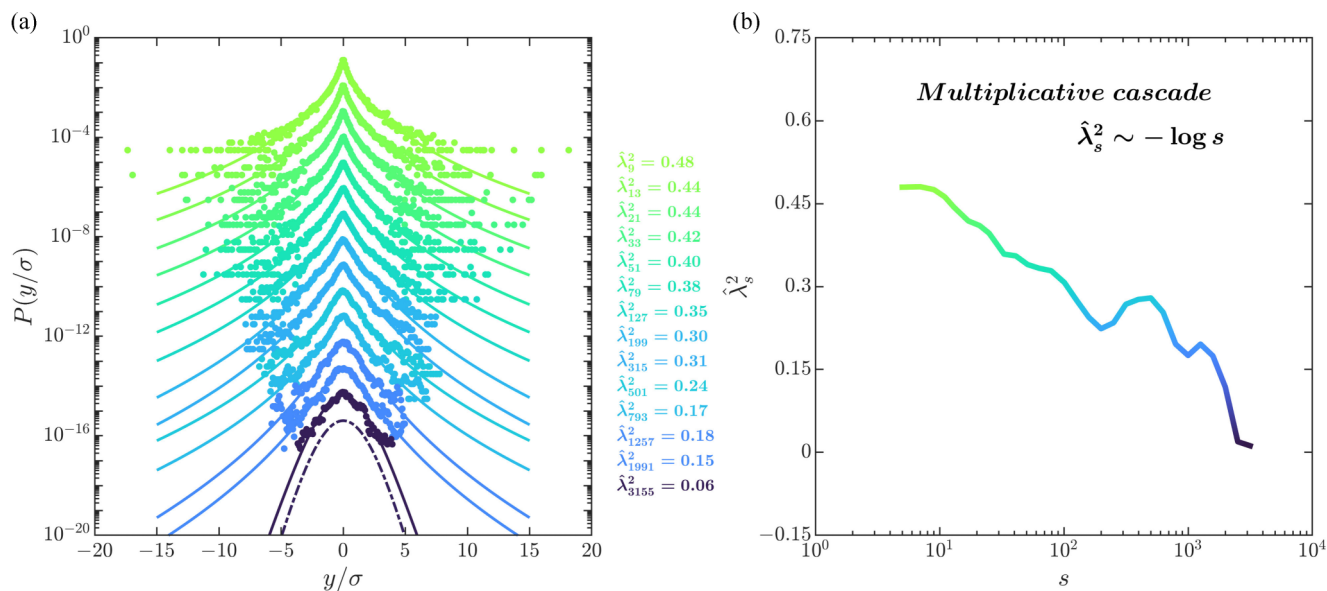
FIG. 5. The multiscale PDF analysis for the multiplicative cascade process. (a) The relationship between non-Gaussianity, $\hat{\lambda}_s^2$, and the shape of the PDF at progressively longer timescales, s, plotted on linear-log coordinates. Solid lines indicate numerical integration of Eq. (2) for the corresponding $\hat{\lambda}^2$ values, while symbols indicate estimated PDFs derived from the standard deviation (SD), $\Delta_s y(t)/\sigma_s$. A dashed line is included to denote a Gaussian distribution for comparison purposes. The PDFs have been vertically shifted for ease of presentation, and thus the vertical axis is provided in arbitrary units. (b) The inverse relationship $\hat{\lambda}_s^2 \sim -\log s$ that is characteristic of cascade-type multiplicative processes. The thick and thin traces represent the relationship between $\hat{\lambda}_s^2$ and $\log s$ for the original cascade series and a shuffled version of the series, respectively.

an even number, while s must be an odd number. One key advantage of the Savitzky-Golay detrending filter is that it can be expressed as a linear convolution, thereby preserving the reproductive property of the normal distribution. Our previous study [88] demonstrated the superior detrending capabilities of the Savitzky-Golay filter compared with other conventional methods: It effectively removes higher-order polynomial trends from the original measurement series (refer also to Refs. [89–91]).

To apply Savitzky-Golay detrending, the smoothly varying component $\tilde{y}_s(t)$ included in the integrated measurement series $y(t) = \sum_{i=1}^{t} x(i)$ is approximated by the Savitzky-Golay smoothing filter and removed from $y(t)$. The increments with timescales s of the integrated time series after detrending are then calculated as

$$\Delta_s y(t) = (y(t+s) - \tilde{y}_s(t+s)) - (y(t) - \tilde{y}_s(t)). \quad (10)$$

Next, using the standardized values of the increments $\Delta_s y(t)$, $\hat{\lambda}^2$ is estimated, as shown in Fig. 5. Notably, $\hat{\lambda}^2 \sim -\ln s$, as derived for the random cascade process in the previous section. Figure 6 shows the sample mean of the moment-based estimator, $\hat{\lambda}_{0.5}^2$, across a range of timescales, s, computed for multiplicative cascades with different theoretical values of λ^2.

Let us delve into the specifics of Gaussian processes to underscore the pivotal role of detrending using the Savitzky-Golay filter in multiscale PDF analysis. Detrending becomes superfluous in the case of nonstationary Gaussian processes devoid of extended trends. In such scenarios, the application of detrending to the time series exerts no discernible influence on the precision of $\hat{\lambda}^2$, especially its dependence on the q exponent [Figs. 7(a)–7(f)]. Conversely, protracted trends in Gaussian processes impact the precision of $\hat{\lambda}^2$, particularly

when examining longer timescales. Thankfully, the utilization of the Savitzky-Golay detrending method enables us to attain a reasonably accurate estimation of $\hat{\lambda}^2$, specifically offering greater stability in the estimation of $\hat{\lambda}^2$ across various q values [Figs. 7(g)–7(l)].
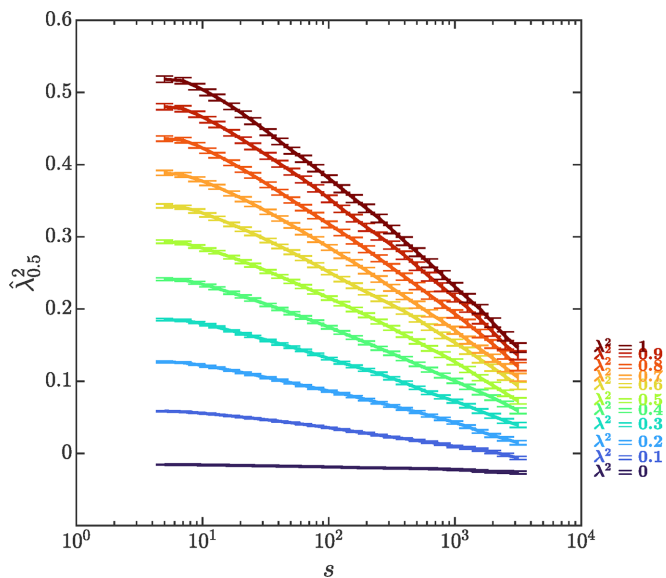

FIG. 6. Sample mean of the moment-based estimator, $\hat{\lambda}_{0.5}^2$, across timescales, s, computed for multiplicative cascades with different theoretical values of λ^2. The sample mean is numerically obtained across 1024 iterations. The error bars indicate the 95% confidence interval.
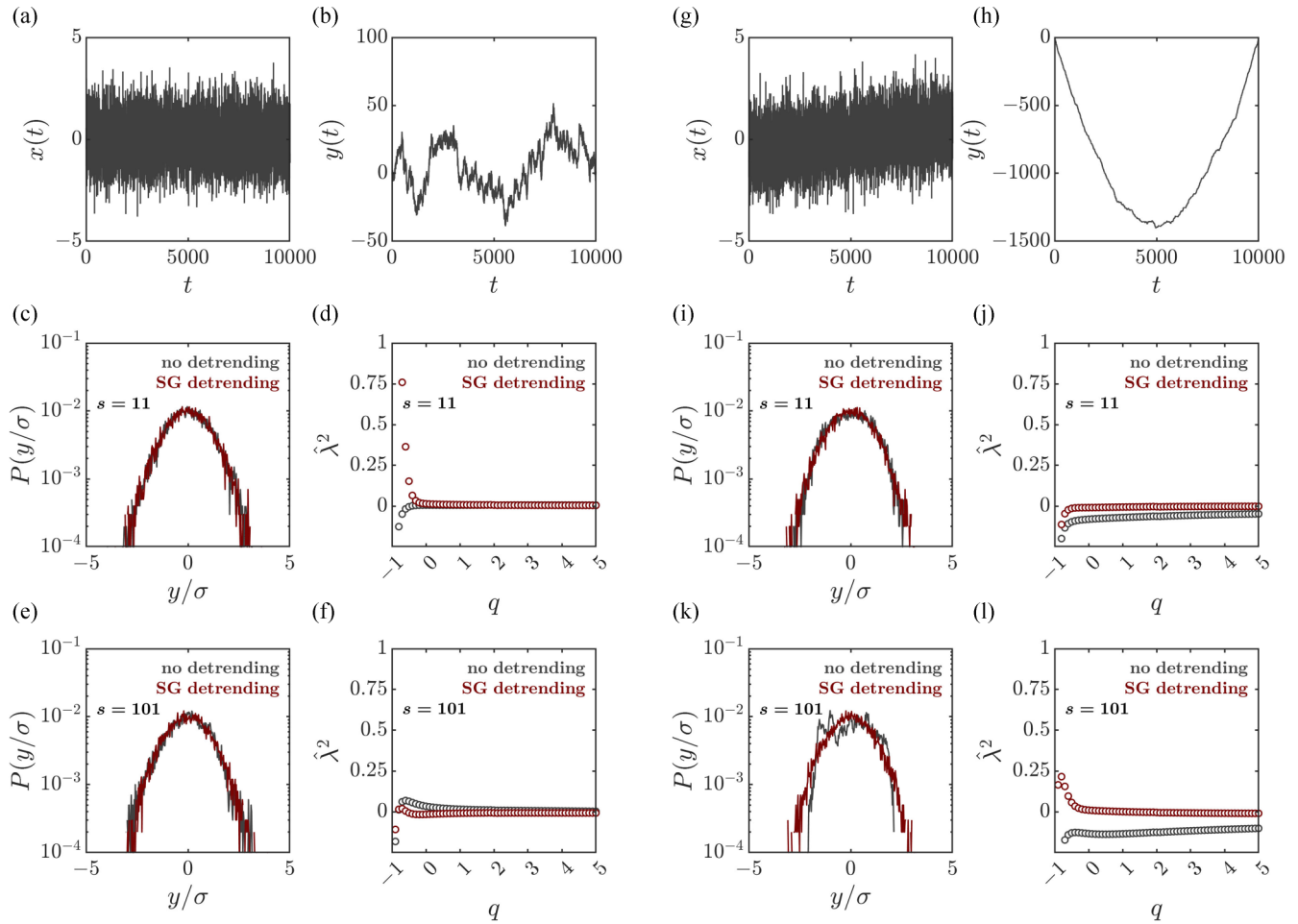
FIG. 7. Detrending the time series is critical for multiscale PDF analysis: The case of Gaussian processes. Long-term trends lead to a less accurate estimation of $\hat{\lambda}^2$, but the Savitzky-Golay (SG) detrending provides a fairly accurate estimation of $\hat{\lambda}^2$. (a) and (b) A nonstationary Gaussian process with no long-term trends and the corresponding integrated time series. (c)–(f) PDF and moment-based estimator of non-Gaussianity $\hat{\lambda}^2$ for the time series in (a) without detrending (gray) and after SG detrending, at timescales $s = 11$ [(c) and (d)] and $s = 101$ [(e) and (f)]. (g) and (h) A nonstationary Gaussian process with a long-term trend and the corresponding integrated time series. (i)–(l) PDF and moment-based estimator of non-Gaussianity $\hat{\lambda}^2$ for the time series in (g) without detrending gray) and after SG detrending, at timescales $s = 11$ [(i) and (j)] and $s = 101$ [(k) and (l)].

Next, let us examine the case of multiplicative cascade processes, which are a natural fit for multiscale PDF analysis. Multiplicative cascades are inherently nonstationary and devoid of long-term trends, rendering detrending unnecessary. Consequently, whether the time series is detrended or not has no bearing on the estimation of $\hat{\lambda}^2$ [Figs. 8(a)–8(f)]. However, when a long-term cascade trend is present in multiplicative cascades, the accuracy of $\hat{\lambda}^2$ diminishes, particularly at longer timescales. Nevertheless, the utilization of the Savitzky-Golay detrending method yields a reasonably accurate estimation of λ^2 [Figs. 8(g)–8(l)]. Despite the challenge posed by the long-term trend in a multiplicative cascade, the Savitzky-Golay detrending technique effectively preserves the accuracy of the estimation.

E. Log-Poisson versus lognormal distributions

The non-Gaussian parameter λ^2 is meaningful when considering the non-Gaussian shape within a multiplicative lognormal distribution framework. However, if the

multiplicative lognormal framework cannot adequately approximate the observed non-Gaussian shape, the q dependence of $\hat{\lambda}_q^2$ is not constant, leading to a more complex interpretation. To delve further into this matter, we examine a log-Poisson cascade process [75,92]. In the log-Poisson cascade process, $\omega^{(j)}$ in Eq. (8) is

$$\omega^{(j)} = C(r, v)\, r P_v, \tag{11}$$

where P_v is an independent Poisson random variable with mean variance v, r is a real-valued parameter, and $C(r, v) = -v(\exp(2r) - 1)/2$. In the case of Poisson processes, the log amplitude from Eq. (4) offers a more interpretable estimation of non-Gaussianity, as illustrated in Fig. 9.

F. Surrogate testing

To ensure that the relationship between $\hat{\lambda}^2$ and $\ln s$ obtained from multiscale PDF analysis accurately reflects cascadelike intermittency, it is crucial to address the issue of nonlinear interactions across scales explicitly. Neglecting this
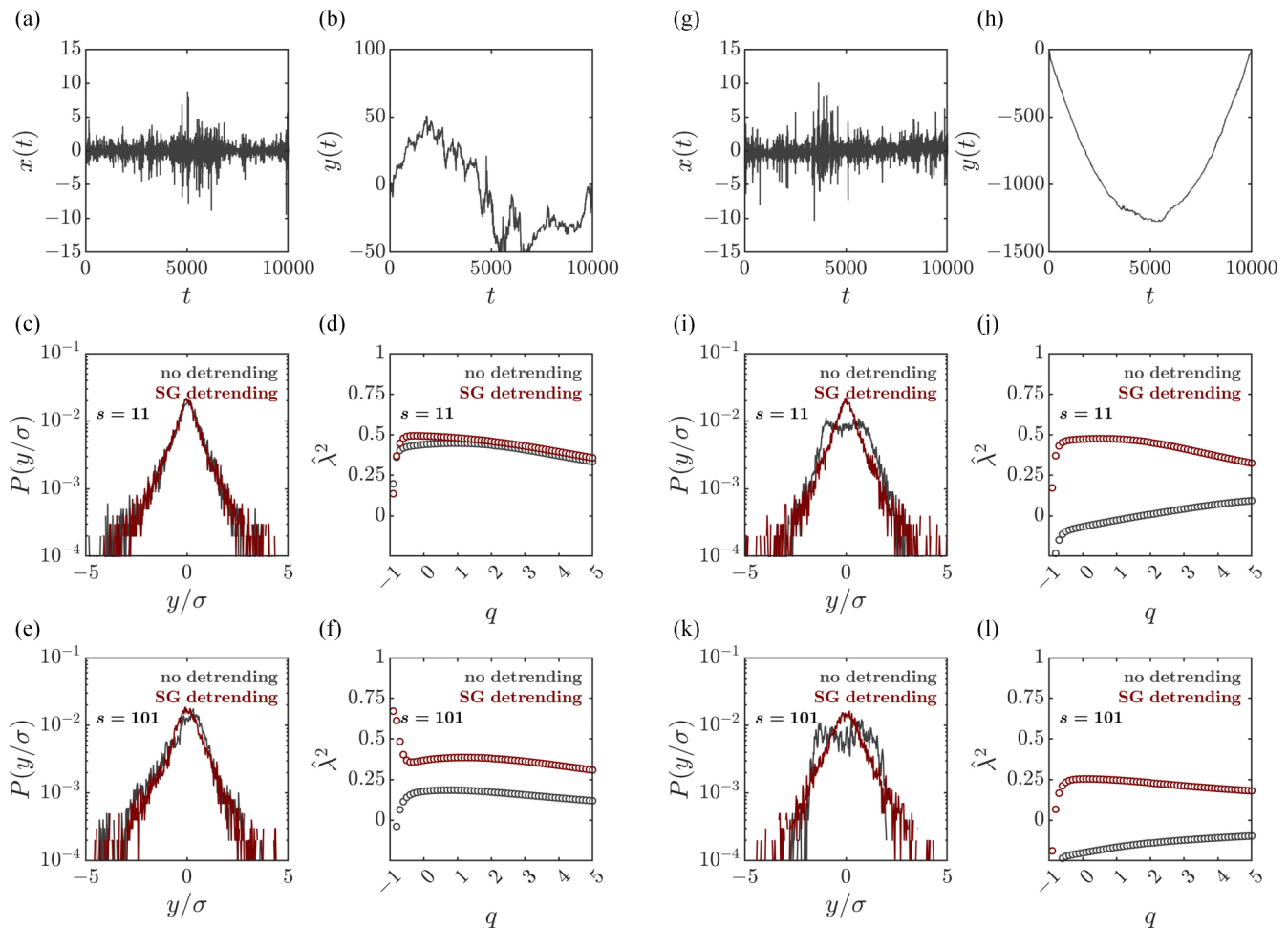
FIG. 8. Detrending the time series is critical for multiscale PDF analysis: The case of multiplicative cascades. Long-term trends lead to a less accurate estimation of $\hat{\lambda}^2$, but the Savitzky-Golay (SG) detrending provides a fairly accurate estimation of $\hat{\lambda}^2$. (a) and (b) A nonstationary cascade process with no long-term trends and the corresponding integrated time series. (c)–(f) PDF and moment-based estimator of non-Gaussianity $\hat{\lambda}^2$ for the time series in (a) without detrending (gray) and after SG detrending, at timescales $s = 11$ [(c) and (d)] and $s = 101$ [(e) and (f)]. (g) and (h) A nonstationary cascade process with a long-term trend and the corresponding integrated time series. (i)–(l) PDF and moment-based estimator of non-Gaussianity $\hat{\lambda}^2$ for the time series in (g) without detrending (gray) and after SG detrending, at timescales $s = 11$ [(i) and (j)] and $s = 101$ [(k) and (l)].

investigation could lead to the same ambiguity encountered in previous treatments of non-Gaussianity. While cascadelike interactivity can generate non-Gaussian patterns, it is important to acknowledge that other mechanisms can also give rise to such patterns, making it challenging to identify cascadelike interactivity definitively. Therefore it is necessary to compare the λ^2-vs-ln s curves for both the original and surrogate series to confirm that the observed non-Gaussianity stems from nonlinear interactions across scales. We recommend employing the well-established iterated amplitude-adjusted Fourier transform (IAAFT) surrogate testing method, which preserves the series' linear autocorrelation and original values. This approach allows us to discern the extent to which the non-Gaussianity observed in the original series can be attributed to cascadelike interactivity and nonlinear temporal correlations relative to the surrogate series. This issue has been extensively discussed in recent studies [69–72], and for further details, readers are encouraged to consult Ref. [93] for comprehensive information on this topic.

In constructing an IAAFT surrogate for a given time series, the initial step involves employing a Fourier transform to separate the series into two distinct components: the amplitude and the phase spectrum. It is worth emphasizing the significance of preserving the amplitude spectrum, which is directly linked to the linear autocorrelation established by the Wiener-Khinchin theorem [94]. Maintaining the integrity of the amplitude spectrum is vital for ensuring the effectiveness of the IAAFT surrogate. These surrogates retain the same linear correlations as the original series by generating a new series that no longer adheres to the original phase sequence.

Subsequently, we introduce randomization to the phase spectrum in the next step. The Fourier-transform phase spectrum establishes a mapping between the phases and their corresponding frequencies in the original time series. By randomizing the phase spectrum, we effectively disrupt this mapping, allowing the same estimated phases to be paired with any available frequency. Notably, the phase spectrum contains residual information about the sequence, which goes
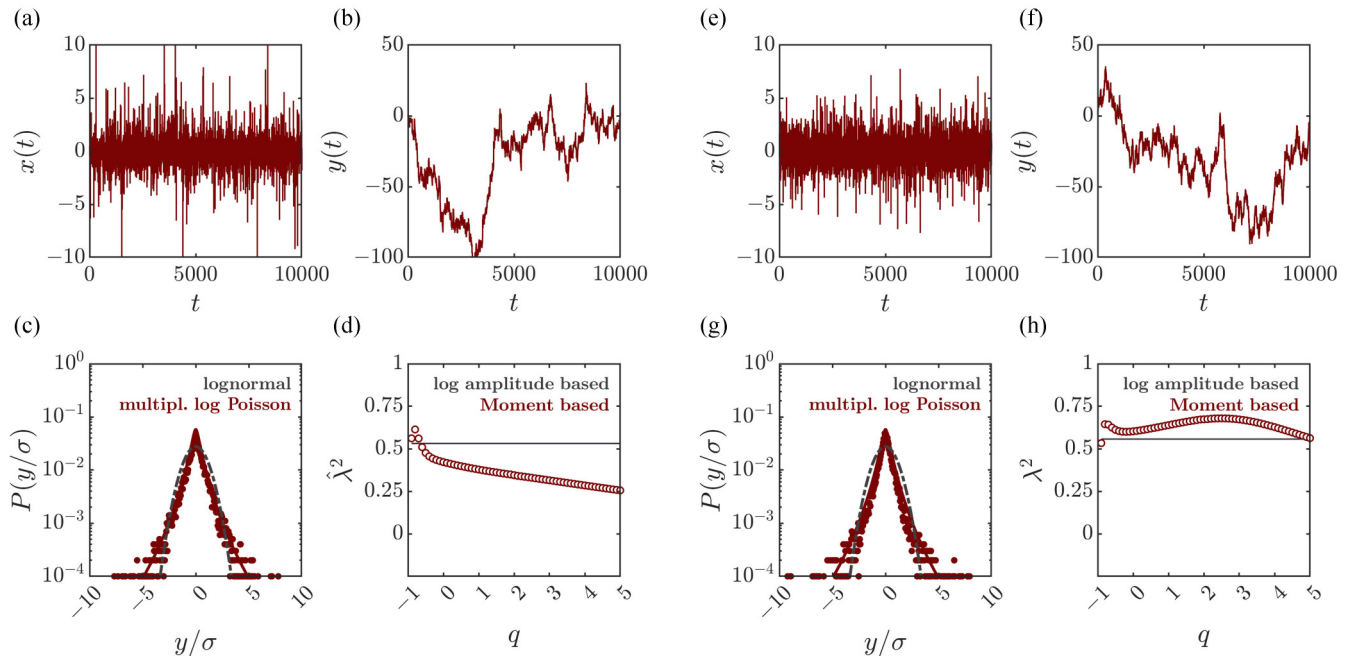
FIG. 9. Two examples showing that $\hat{\lambda}^2$ is the parameter of the lognormal model. If a time series does not conform to this model, interpreting $\hat{\lambda}^2$ becomes meaningless. In such cases, we can use the log amplitude from Eq. (4) as a comparable measure of non-Gaussianity. (a) and (e) Time series from a non-Gaussian process called the log-Poisson model. (b) and (f) Integrated time series. (c) and (g) PDF of the time series. (d) and (h) Log-amplitude- and moment-based estimators of non-Gaussianity, with the moment-based estimator computed for a range of qth-order absolute moments. Here, multipl., multiplicative.

beyond what the linear autocorrelation can fully explain as it also encompasses nonlinear correlations. In contrast, the amplitude spectrum primarily captures the linear correlations inherent in the time series.

In the third step, we perform an inverse Fourier transform on both the original amplitude and the randomized phase spectrum. This process generates a random time series that has not been previously measured but possesses identical linear correlations to the original time series. It is crucial to recognize that while this new time series shares the same linear correlations, it lacks the original nonlinear correlations due to the randomization of the phase spectrum on which it is based. The similarity between this inverse Fourier transform and the original measurement series is limited to their linear correlations alone. Consequently, additional steps are necessary to reintegrate the original measured values into this similarly structured linear correlation framework.

In the fourth step, the IAAFT surrogate is carefully aligned with the histogram of the original series. This involves replacing the original values with those from the inverse Fourier series while maintaining their linear correlations. The IAAFT method ranks both series, sorting the values from largest to smallest, and subsequently replaces the jth-ranked value of the inverse Fourier series with the corresponding jth-ranked value of the original series. This rank-based replacement procedure ensures that the surrogate series accurately reflects the peaks and valleys of the original series, thereby preserving its linear correlations. By undergoing this step, we inch closer to achieving a linear approximation of the original series. The surrogate series retains the linear autocorrelation obtained in the previous step and reinstates the original values, including their mean and variance.

In the final step, the IAAFT method produces an iterative convergence process that gradually refines the surrogate series toward the original series. The researcher has the flexibility to choose a benchmark that determines the desired level of similarity between the final IAAFT surrogate and the amplitude spectrum of the original series. It is essential to acknowledge that the preceding rank-matched replacement step might have altered the amplitude spectrum, notably if the histogram of the original series deviates from a Gaussian distribution. For instance, the surrogate inverse Fourier series may exhibit more pronounced peaks in heavy-tailed distributions. Conversely, suppose there is an overabundance of small values near zero. In that case, the valleys in the inverse Fourier series might become shallower following rank matching, potentially distorting the representation of oscillations in the original series. In cases where the convergence of the IAAFT process is not achieved, the software continues iterating until the maximum number of specified iterations is reached.

In summary, surrogate testing addresses the crucial issue of nonlinear interactions across scales inherent in cascade-like interactivity. While multiscale PDF analysis primarily focuses on capturing the non-Gaussian patterns associated with cascadelike intermittency, surrogate testing enhances the empirical evidence of cascadelike intermittency by examining the presence of nonlinearity. Through the IAAFT procedure, a new time series is generated, replicating the amplitude spectra and preserving the linear autocorrelation while disrupting the phase spectra, indicating potential nonlinear interactions across scales in the original sequence. For each measurement series, we can generate a set of surrogate series representing likely linear models of the original series. By comparing the non-Gaussianity of the original series with that of the
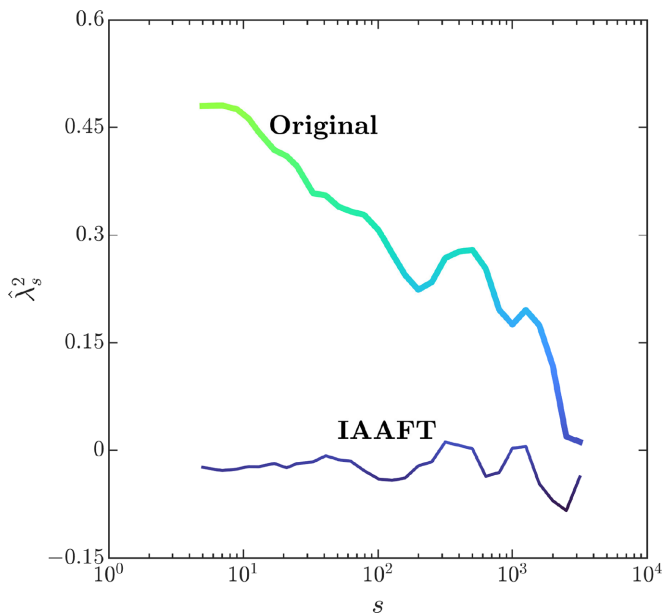
FIG. 10. IAAFT surrogate analysis allows one to determine whether the observed $\hat{\lambda}^2$-vs-ln s curve can be explained by cascadelike interactivity. By comparing the $\hat{\lambda}^2$ values estimated for the original series with those of the corresponding IAAFT surrogate at a given timescale, we can determine the extent to which cascadelike interactivity contributes to non-Gaussianity relative to linear sources for that timescale.

surrogate series using a one-sample t-test, we can detect the presence of nonlinearity. As illustrated in Fig. 10, the discrepancy in the estimated $\hat{\lambda}^2$ values between the original time series and the corresponding IAAFT surrogate at a specific timescale indicates the contribution of cascadelike interactivity over linear sources of non-Gaussianity for that particular timescale. This approach provides valuable insights into the interplay between the analyzed system's nonlinear interactions and cascade dynamics.

V. APPLICATIONS OF MULTISCALE PDF ANALYSIS

A. Heart rate variability in congestive heart failure

We conducted a multiscale PDF analysis on the long-term ambulatory heart rate variability (HRV) data of 280 individuals, comprising 69 patients with congestive heart failure (CHF) who survived (mean $\pm$ SD age, 64 ± 15 yr; 27 women), 39 patients with CHF who did not survive (70 ± 14 yr; 20 women), and 115 healthy adults (47.7 ± 18.2 yr; 25 women). The primary end point of our study was all-cause mortality, with the majority of deaths (34 out of 39) attributed to heart-related causes. We obtained the data from previously published studies [64]. Figures 11(a)–11(c) display the R-R interval (R-wave peak to R-wave peak; RRi) time series $x(t)$ of a healthy subject and two patients with CHF (one survivor and one nonsurvivor), while Figs. 11(d)–11(f) represent the same data after detrending at three distinct timescales. The PDF curves of the healthy subject remained relatively consistent across all timescales [Fig. 11(g)]. Conversely, the PDF curves for patients with CHF exhibited more tapered centers and fatter tails at smaller scales [Figs. 11(h) and 11(i)],

indicating greater intermittent deviations at shorter timescales. Additionally, as the timescale increased, we observed a rapid convergence of the PDFs towards a Gaussian distribution solely among patients with CHF.

The deformation of the non-Gaussian PDF can be elucidated by examining the relationship between the estimator $\hat{\lambda}^2_s$ and timescale s. While all groups exhibit a general linear decrease from the peak in $\hat{\lambda}^2_s$, the groups primarily differ in peak height and timescale. Healthy subjects show minimal variation in $\hat{\lambda}^2$ across a wide range of timescales, resulting in an almost zero value of the $\hat{\lambda}^2$-vs-ln s slope over shorter timescales. The peak in $\hat{\lambda}^2$ occurs around $s = 10$–20 s, followed by a gradual decline across medium to longer timescales. In contrast, patients with CHF, particularly nonsurvivors with sympathetic overdrive, exhibit considerably higher peaks around $s = 10$–20 s. As the timescale surpasses 20 s, the decrease in $\hat{\lambda}^2$ follows an almost linear decay for both CHF groups, with a more monotonic decline in nonsurviving patients with CHF. Notably, this pattern resembles that observed in the cascade model of intermittent turbulence. Hence, if we disregard the specific timescale and peak height and focus solely on the linear slopes, the $\hat{\lambda}^2$-vs-ln s slope for patients with CHF would be notably more negative than that for healthy controls. Specifically, the negative non-Gaussianity estimates of HRV in patients with CHF with sympathetic overdrive, decaying within the 20–200-s timescale range, suggest a sympathetic origin for HRV intermittency: During these timescales, HRV reflects cardiovascular regulation influenced by neural and humoral factors [73].

Figure 12 clearly shows that the $\hat{\lambda}^2_{25}$ for patients with CHF is slightly but significantly higher [mean $\pm$ standard error of the mean (SEM) = 0.39 ± 0.030] than that of healthy controls (0.19 ± 0.014, $t_{278} = 8.30$, $p < 0.001$). Additionally, λ^2_{25} is significantly higher for patients with CHF who did not survive (0.48 ± 0.057) than for those who survived (0.35 ± 0.033, $t_{106} = 2.15$, $p = 0.034$). Because $\hat{\lambda}^2_{25}$ for the corresponding surrogate RRi time series did not differ among the three groups ($p > 0.05$), the differences between these groups can be attributed to differences in cascadelike interactivity in HRV rather than linear sources of non-Gaussianity. Lower values of λ^2_{25} can be used as a proxy for healthy cardiovascular functioning, as previously reported in patients with acute myocardial infarction (AMI) taking (antisympathetic) beta blockers [95].

Recognizing that physiological time series may deviate from the conventional patterns observed in theoretical cascade simulations holds significant importance. For instance, in the case of HRV, a relatively Gaussian pattern is observed at shorter timescales, while stronger non-Gaussianity emerges at longer timescales. Non-Gaussianity may intensify with timescales due to the inherent capacity of physiological processes to exploit or manifest constraints. In the context of healthy HRV, we observe a gradual increase in non-Gaussianity over shorter timescales, potentially reflecting the influence of constraints that regulate non-Gaussian behavior. However, in the presence of CHF, the nonmonotonic nature of non-Gaussianity becomes more pronounced. CHF leads to an elevation in the peak of non-Gaussianity, positioning it predominantly at the shortest timescales. Consequently, if physiological time series exhibit nonmonotonic
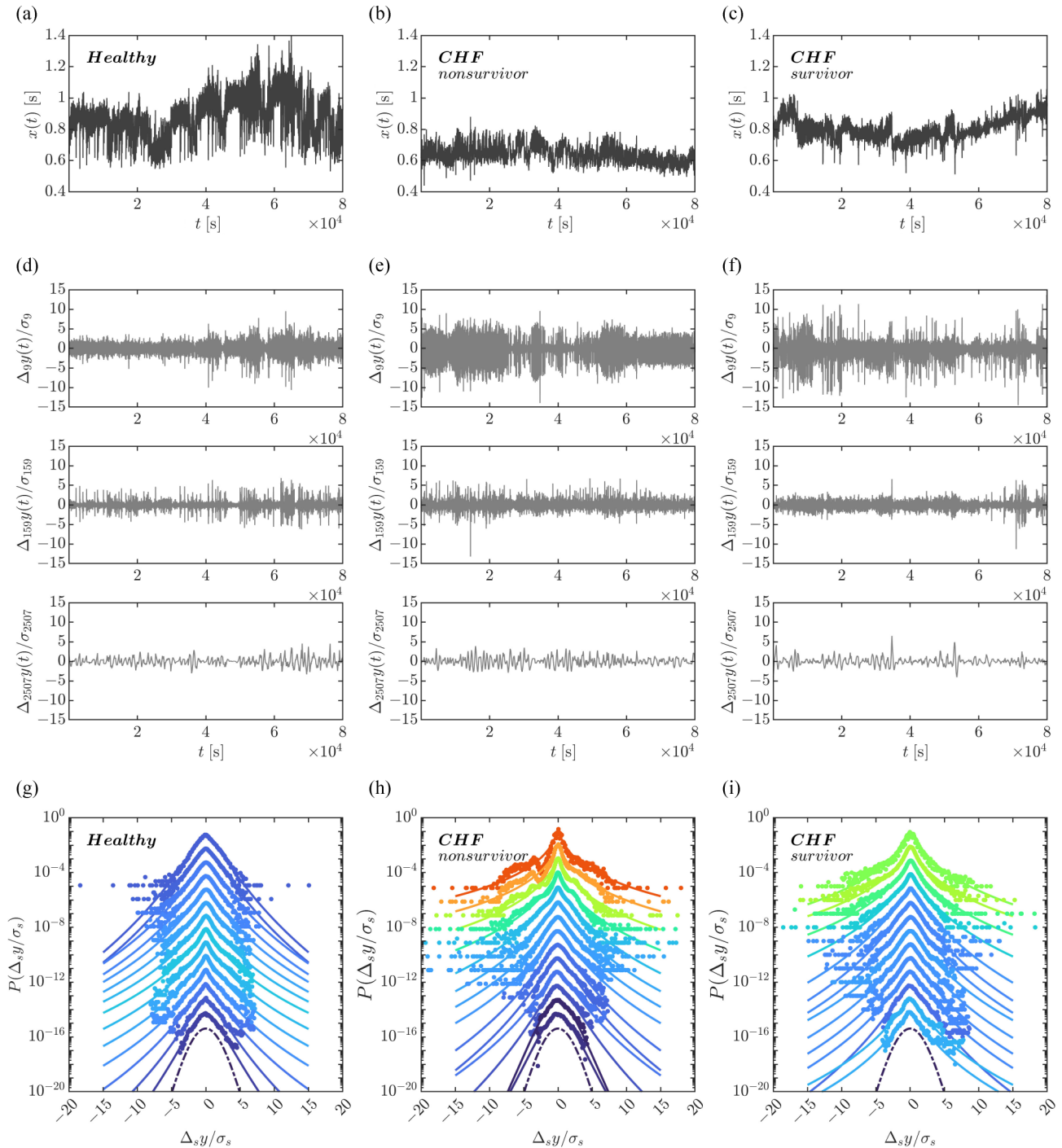
FIG. 11. Multiscale PDF characterization of heart rate variability. (a)–(c) Representative examples of time series of nearest-neighbor intervals $b(t)$. (d)–(f) Time series of $\Delta_9 y(t)/\sigma_9$ (top), $\Delta_{159} y(t)/\sigma_{159}$ (middle), and $\Delta_{2507} y(t)/\sigma_{2507}$ (bottom). (g)–(i) Standardized PDFs (in logarithmic scale) of $\Delta_s y(t)/\sigma_s$ (from top to bottom) for $s = 7, 11, 17, 25, 41, 63, 101, 159, 251, 397, 629, 999, 1581, 2507$ s, where σ_s denotes the SD of $\Delta_s y(t)$. Solid lines indicate numerical integration of Eq. (2) for the respective λ^2 values. Symbols indicate estimated PDFs from the time series shown in (d)–(f). The PDFs have been shifted vertically for the convenience of presentation; thus the vertical axis is given in arbitrary units. The left panels [(a), (d), and (g)] are data for a healthy individual (a 45-yr-old man). The center panels [(b), (e), and (h)] are data for a 66-yr-old woman with congestive heart failure (CHF) who died 60 days after the measurement. The right panels [(c), (f), and (i)] are data for an 82-yr-old woman who survived CHF.

behaviors, such as the presence of peaks, it becomes beneficial to supplement the fitting of simple linear slopes with a careful assessment of peak height and location. Identifying specific timescales at which healthy and stable functioning constraints give way to non-Gaussianity could potentially hold diagnostic value [64]. This ability of the multiscale PDF analysis to provide valuable insights even when the changes in non-Gaussianity with timescale deviate from the canonical
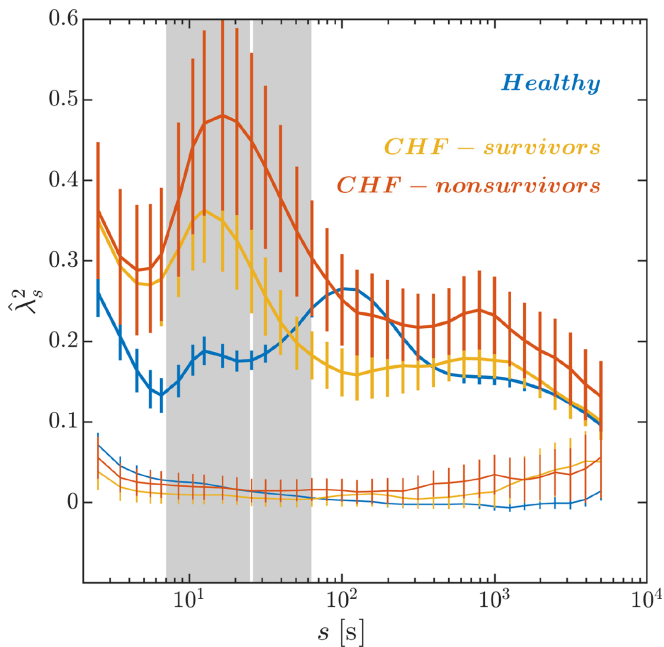
FIG. 12. Timescale dependence of the non-Gaussianity parameter $\hat{\lambda}^2$ for the original HRV series (thick lines) and their corresponding IAAFT surrogates (thin lines). The results are for patients with congestive heart failure (CHF), both for the survivors ($n = 69$) and nonsurvivors ($n = 39$). Age-matched controls were selected from a database of healthy subjects ($n = 172$). Error bars indicate 95% confidence intervals of the group averages. The gray patch covers the timescales, s, for which $\hat{\lambda}^2$ differs across the three groups, and the white vertical line indicates $s = 25$ s.

expectations derived from cascade modeling highlights its versatility and applicability beyond the confines of traditional cascade-modeling paradigms.

B. Postural sway in Parkinson's disease

Our daily tasks often require us to stand upright, feet firmly planted on the ground, while keeping our focus on a target. Although seemingly straightforward, this action involves a sophisticated interplay of perceptual and motor processes that span various levels of complexity. At a finer scale, mechanoreceptors detect joint angles, photoreceptors respond to light stimuli, and ocular muscles work in tandem to maintain a stable visual image. Zooming out to a larger scale, we encounter higher-order structures with visual and mechanical information intertwined, resulting in an immersive pattern of data, such as optic flow. Within this medium scale, a hierarchical system of reflex arcs comes into play, coordinating with muscle groups to create synergies, all under the supervision of a central executive that plans activities and provides sensory correction. This cascade becomes evident in the postural center of pressure (CoP), where the body's mechanical pressures converge on the ground: The upright stance presents a web of interdependent factors that support the engagement of our once-stationary bodies with the surrounding world. This cascade-dynamical structure can be observed in the CoP and provides multiscaled sensitivity, enabling us to carry out planned activities with precision and adaptability [96–103].

We conducted a multiscale PDF analysis on the Euclidean displacement series of the CoP obtained from a sample of 32 individuals with Parkinson's disease (mean ± SD age, 66 ± 10 yr; 8 women) in both on-medication and off-medication conditions, 22 healthy older adults (67 ± 8 yr; 11 women), and 27 healthy younger adults (28 ± 5 yr; 12 women). The CoP data, collected at a rate of 100 Hz, were acquired from publicly available data sets [104,105]. During the experiment, participants maintained a stable upright stance with their eyes open for 30 s. Figures 13(a)–13(c) display the time series of Euclidean displacements in the CoP for a representative healthy young adult, healthy older adult, and patient with Parkinson's on medication. Figures 13(d)–13(f) represent the same data after detrending at three distinct timescales. Both healthy young adults and healthy older adults exhibited a similar deviation from the Gaussian distribution at shorter and longer timescales, gradually converging towards a Gaussian form in the medium timescales [Figs. 13(g) and 13(h), respectively]. In stark contrast, individuals with Parkinson's disease on medication consistently displayed a non-Gaussian form in postural sway across all timescales, indicating significant intermittent deviations or bursts in postural sway at shorter timescales [Fig. 13(i)].

The distinction in the estimator $\hat{\lambda}^2$ between healthy adults and individuals with Parkinson's disease became evident primarily in the shortest timescales (Fig. 14). Individuals with Parkinson's disease exhibited a substantial increase in $\hat{\lambda}^2$ compared with their healthy counterparts, irrespective of age or medication status. The $\hat{\lambda}^2$-vs-ln s curves for the surrogate series did not display this trend, indicating that the observed differences stemmed from variations in cascadelike interactivity rather than linear sources of non-Gaussianity. These findings underscore the capability of multiscale PDF analysis in discerning clinical disparities in postural sway. Furthermore, they shed light on the contrasting nature of non-Gaussianity profiles across multiple timescales between Parkinson's disease and healthy aging.

C. Postural sway across task constraints

While the previous example showcases the potential of multiscale PDF analysis in discerning clinical disparities, it is essential to note that empirical measurements of clinical differences can sometimes be exaggerated and highly dependent on the specific analysis employed. The discrepancies between clinical and healthy populations can be so pronounced that any analysis will likely yield noticeable distinctions. To highlight the sensitivity of multiscale PDF analysis to more subtle variations in intermittency in physiology, we showcase another example that delves into the realm of healthy upright standing, where the range of variation is narrower and more nuanced.

The previous example involving postural CoP emphasized the significance of intermittency, a widely recognized characteristic of postural control [69–72,100,106–108]. Intermittency refers to statistical instability or unevenness observed over time or space and, despite its counterintuitive nature, is considered crucial for maintaining an upright stance. However, an ongoing debate persists regarding the underlying control mechanisms responsible for generating intermittency. One perspective posits that intermittency arises from discrete
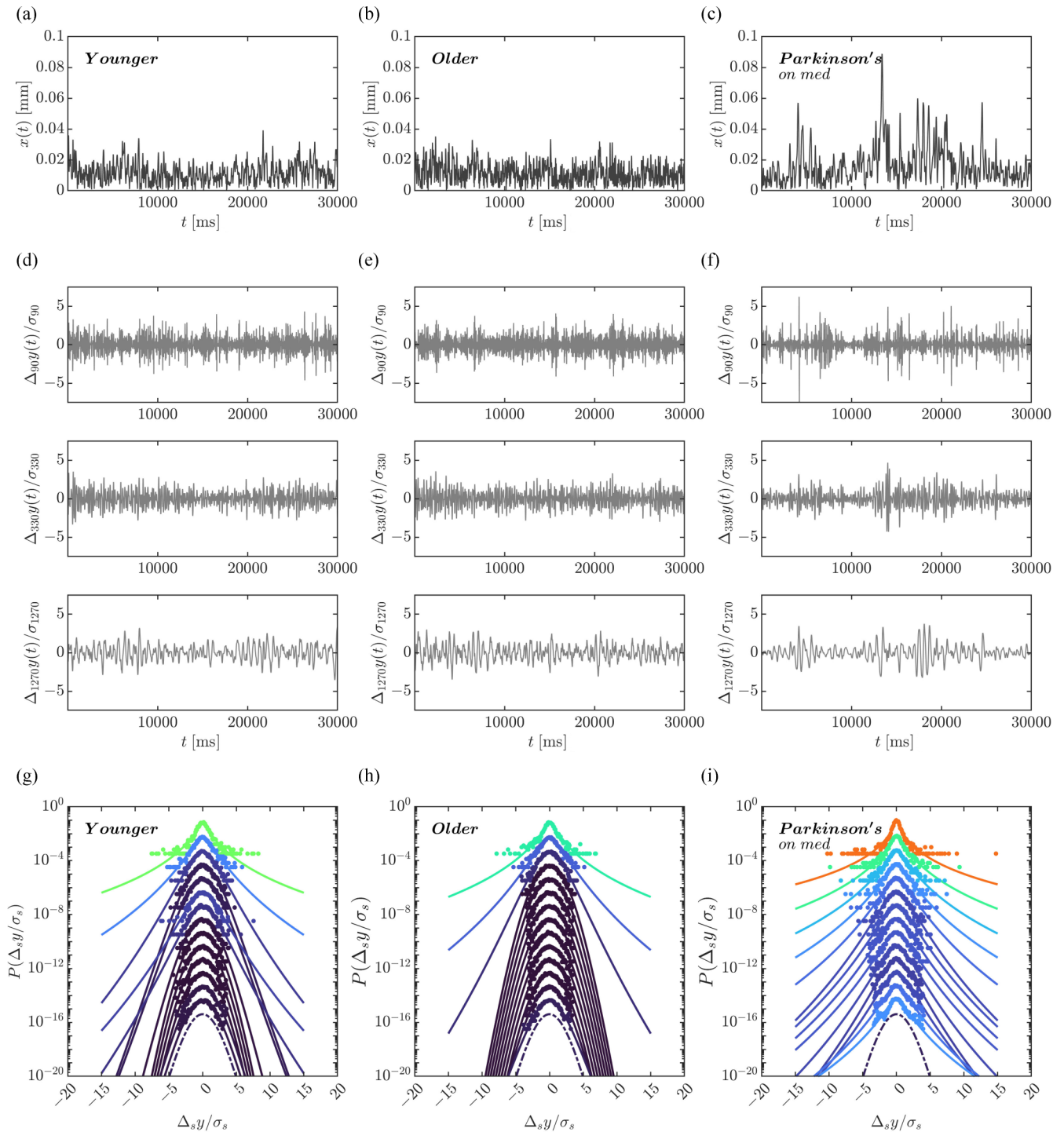
FIG. 13. Multiscale PDF characterization of postural CoP in individuals with Parkinson's disease and age-matched healthy controls. (a)–(c) CoP Euclidean displacement time series $b(t)$. (d)–(f) Detrended $\Delta_{90}y(t)/\sigma_{90}$ (top), $\Delta_{330}y(t)/\sigma_{330}$ (middle), and $\Delta_{1270}y(t)/\sigma_{1270}$ (bottom). (g)–(i) Standardized PDFs of $\Delta_{s}y(t)/\sigma_{s}$ (top to bottom) for $s = 7, 11, 17, 25, 41, 63, 101, 159, 251, 397, 629, 999, 1581, 2507$ ms, where σ_{s} is the SD of $\Delta_{s}y(t)$. Solid lines show numerical integration of Eq. (2) for $\hat{\lambda}^2$ values. Symbols represent estimated PDFs from the time series in (a), with vertical shifting for clarity. The left panels [(a), (d), and (g)] show data for a healthy younger adult: a 24-yr-old woman. The center panels [(b), (e), and (h)] are data for a healthy older adult: a 63-yr-old man. The right panels [(c), (f), and (i)] show data for a patient with Parkinson's on medication (med): a 70-yr-old woman.

switching between different control modes, where constraints on sway engagement or disengagement play a mediating role [109–113]. According to this viewpoint, constraints are disengaged when the sway is minimal and poses no immediate threat to upright stability, resulting in increased variability in sway. Randomness in sway implies a stochastic sequence of constraint engagement and disengagement, leading to a short-lag negative autocorrelation amidst uncorrelated variability.
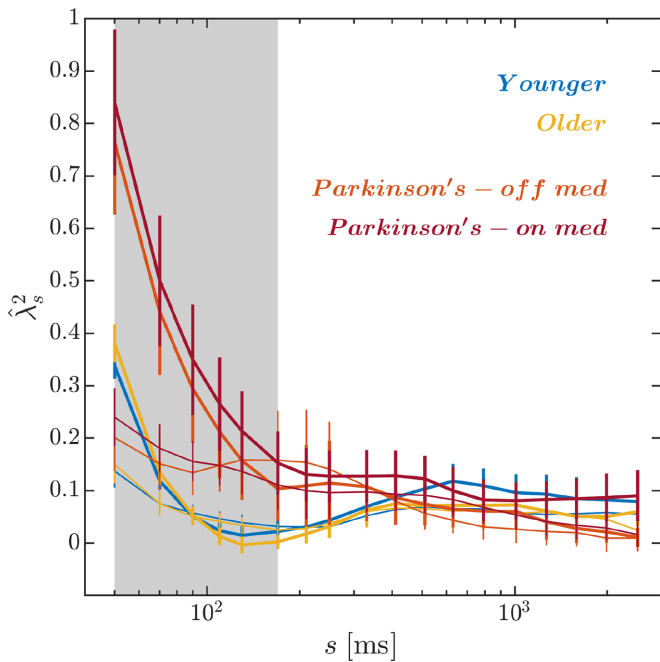
FIG. 14. Non-Gaussianity, $\hat{\lambda}^2$, vs timescale, s, for original CoP Euclidean displacement series (thick lines) and their IAAFT surrogates (thin lines) for younger and older adults, as well as individuals with Parkinson's disease on and off medication while standing upright with eyes open. The error bars represent 95% confidence intervals of the group averages. The gray patch indicates the timescales with different $\hat{\lambda}^2$ between healthy adults (younger and older) and individuals with Parkinson's disease.

This type of intermittency exhibits less of a cascadelike behavior and is less suitable for multiscale PDF analysis [71].

The alternative interpretation of intermittency in postural control, which portrays feedback-based corrections as unfolding in a cascading manner across various timescales, offers a more nuanced understanding, as postural control can exhibit two distinct behaviors: "trembling" around equilibrium points and "rambling," where shifts occur between different equilibrium points [114,115]. Rambling entails the integration of diverse information and necessitates active mechanical processes [116–118]; passive reflex mechanisms [119,120]; and anticipatory [121–123], feedback [124,125], and exploratory responses [126,127]. Coordinating all these information sources across different spatial and temporal scales requires a precise cascade structure, to which the multiscale PDF analysis is uniquely attuned [72,128].

This illustration highlights how multiscale PDF analysis enriches our understanding of the role of cascade dynamics in postural control. This method is crucial in capturing the scale-dependent structure of cascade dynamics, which is vital in coordinating corrective movements. For instance, postural corrections may exhibit a cascadelike pattern or negative short-lag autocorrelation. However, this cascade must vary across scales and reflect the boundary at which postural control transitions to feedback-based control. During short-scale postural sway, fluctuations occur freely within the base of support, resulting in low λ values that increase at certain timescales before eventually declining, resembling the

behavior of a cascade. In the case of a relatively stable stance, the $\hat{\lambda}^2$-vs-log s curve should exhibit a quadratic shape. However, destabilizing the support surface or closing one's eyes diminishes the scale dependence of λ, prompting a search for new equilibrium points and leading to a linear decay akin to scale-invariant cascades. Therefore multiscale PDF analysis provides valuable insights into the significance of scale-dependent structure in postural control and the critical role of cascade dynamics in this intricate process.

We performed PDF analysis on the CoP Euclidean displacement series of 22 older adults (mean $\pm$ SD age, 67 ± 8 yr; 11 women) and 27 healthy younger adults (28 ± 5 yr; 12 women) standing upright under three distinct conditions: (i) eyes open on a rigid surface, (ii) eyes open on a foam sheet, and (iii) eyes closed on a foam sheet. The data used for this analysis were obtained from a publicly available data set [104]. Figures 15(a)–15(c) depict the time series of Euclidean displacements in the CoP for a representative older adult in the three conditions above standing upright with eyes open on a rigid surface, eyes open on a foam sheet, and eyes closed on a foam sheet. Figures 15(d)–15(f) represent the same data after detrending at three distinct timescales. When standing on a rigid surface with eyes open, postural sway exhibited a PDF with a similar deviation from the Gaussian form at both shorter and longer timescales, gradually converging towards the Gaussian form at medium timescales [Fig. 15(g)]. However, when standing on a foam sheet with eyes open or closed, postural sway exhibited significant intermittent deviations or bursts at shorter timescales, resulting from the introduction of novel task constraints that can destabilize posture [Figs. 15(h) and 15(i)].

The λ^2-vs-ln s curves revealed notable distinctions between younger and older adults in all three task conditions, with the most significant differences observed at the shortest timescales, where the introduction of novel task constraints can trigger intermittent deviations or bursts in postural sway (Fig. 16). These findings demonstrate the effectiveness of multiscale PDF analysis in identifying the boundary where postural control can naturally fluctuate and the point at which it necessitates feedback-based control. Furthermore, this analytical approach proves equally valuable in discriminating between clinical-patient populations and healthy populations and detecting subtle variations in healthy upright standing.

VI. DISCUSSION

This work explains the multiscale PDF analysis for quantifying non-Gaussian intermittent physiological fluctuations. While non-Gaussianity is a known empirical characteristic of intermittent fluctuations in physiology, its assessment has been ambiguous, mainly based on the heaviness of PDF tails. Additionally, PDF tails provide inadequate support for parameter estimation due to small-sample bias and the inability to represent nonlinear correlations or polynomial trends. Multiscale PDF analysis overcomes many existing limitations by modeling the better-populated portion of the PDF using lognormal variance, modifying this variance by detrending the underlying sequence, and examining how this detrended lognormal variance grows with scales. In summary, multiscale PDF analysis is a promising new approach for studying
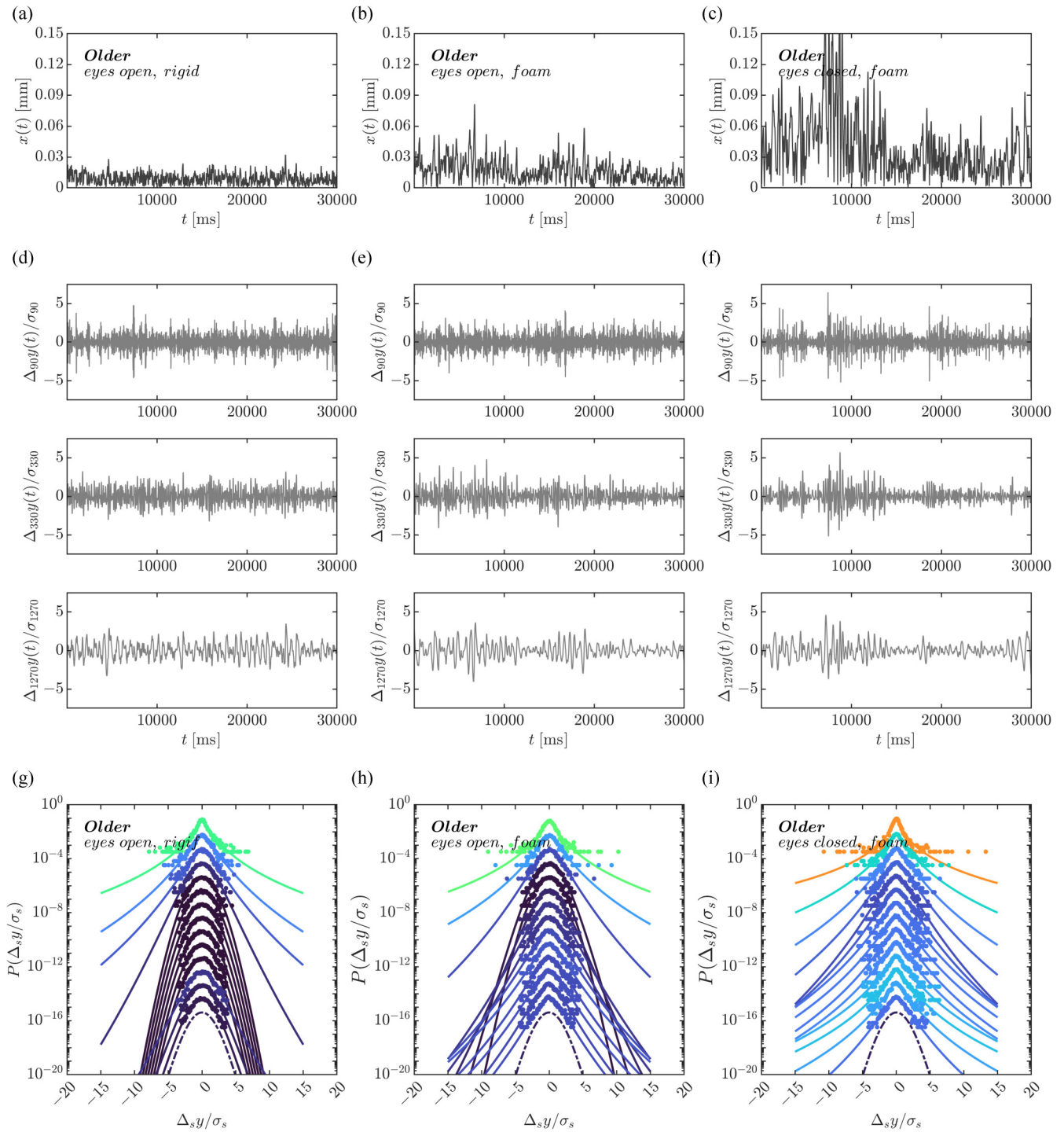
FIG. 15. Multiscale PDF characterization of postural CoP in an older adult (63-yr-old man) standing upright with eyes open on a rigid surface [left panels: (a), (d), and (g)], eyes open on a foam sheet [middle panels: (b), (e), and (h)], eyes closed on a foam sheet [right panels: (c), (f), and (i)]. (a)–(c) CoP Euclidean displacement time series $b(t)$. (d)–(f) Detrended $\Delta_{90}y(t)/\sigma_{90}$ (top), $\Delta_{330}y(t)/\sigma_{330}$ (middle), and $\Delta_{1270}y(t)/\sigma_{1270}$ (bottom). (g)–(i) Standardized PDFs of $\Delta_s y(t)/\sigma_s$ (top to bottom) for $s = 7, 11, 17, 25, 41, 63, 101, 159, 251, 397, 629, 999, 1581, 2507$ ms, where σ_s is the SD of $\Delta_s y(t)$. Solid lines show numerical integration of Eq. (2) for $\hat{\lambda}^2$ values. Symbols represent estimated PDFs from the time series in (a), with vertical shifting for clarity.

intermittent fluctuations in physiology, offering a powerful new avenue for empirical applications.

We have thoroughly explained the multiscale PDF analysis from theoretical and empirical perspectives. Theoretically, we

have introduced the algorithm for the analysis and elaborations to ensure greater generality of results. For example, the traditional approach of using lognormal variance is best suited for the lognormal model. However, to extend to alternative
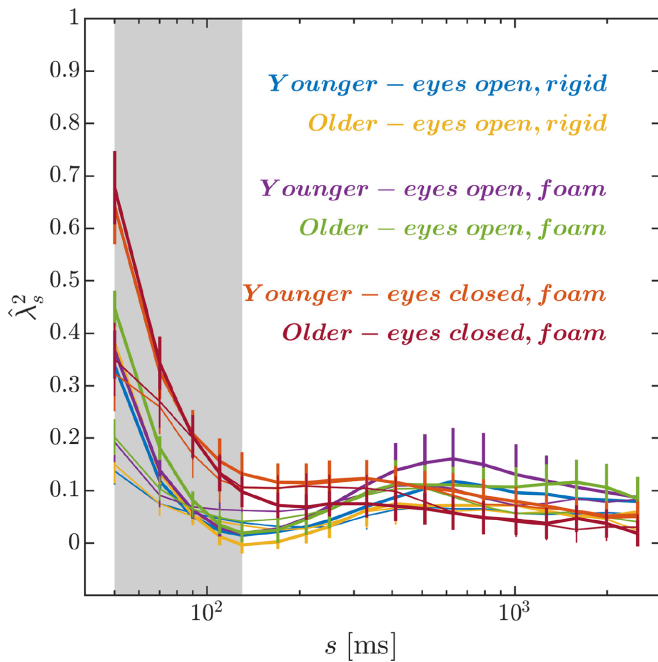
FIG. 16. Non-Gaussianity, $\hat{\lambda}^2$, vs timescale, s, for original CoP Euclidean displacement series (thick lines) and their IAAFT surrogates (thin lines) for younger and older adults standing upright with eyes open on a rigid surface, eyes open on a foam sheet, and eyes closed on a foam sheet. The error bars represent 95% confidence intervals of the group averages. The gray patch indicates the timescales with different $\hat{\lambda}^2$ between healthy adults and older individuals.

models such as the log-Poisson model, we have derived a log-cumulant approach that may be more resilient for a broader range of processes. We have utilized simulation data to determine the best practices for selecting measurement series' lengths and timescales. Additionally, we have examined detrending as it may remain a challenging issue for measurement series with increasingly longer-term trends.

We have elucidated the application of the multiscale PDF analysis in conjunction with surrogate testing. This step assumes paramount importance due to the potential influence of detrending challenges on non-Gaussianity estimates, which could inadvertently reflect linear temporal correlations. Consequently, employing surrogate series to validate that the observed non-Gaussianity signifies nonlinear temporal correlations becomes indispensable. Although non-Gaussianity is a vital characteristic of cascadelike interactivity, it does not exclusively define it. The concept of "polydispersity" in the literature, which quantifies heterogeneity and variety, has underscored that non-Gaussianity becomes a genuine hallmark of cascadelike interactivity only when it coexists with and logically follows nonlinear correlations, thereby serving as a predictive factor [129].

Regarding empirical applications, we have illustrated that congestive heart failure and postural control instability during upright standing exhibit strong linear decays in $\hat{\lambda}^2$, consistent with traditional predictions from the cascade-theoretic scholarship. Of course, physiological dynamics under various constraints, whether from measurement circumstances or systemic weakness, may not fully conform to the canonical expectations from cascade-based theorizing across all timescales. Nonetheless, we have suggested potential ways in which the nonmonotonicities in $\hat{\lambda}^2$-vs-log s relationships could provide diagnostic information about the cascadelike interactivity underlying healthy functioning [101,130–134].

The human body operates as a complex network of interconnected physiological systems that interact continuously to coordinate functions and maintain health. These interactions happen at various levels and timescales, involving synchronized activities and signaling pathways [135–139]. It is not enough to merely have well-functioning individual systems. It is equally vital to ensure their seamless interaction for healthy functioning. Any disruption in the coordination between these systems can result in dysfunction or even complete organ failure, as evidenced in sepsis and multiple organ failure [140–143]. Despite advancements in systems biology and integrative physiology, we still lack a comprehensive understanding of how these diverse systems interact and integrate to produce physiological states in health and disease. The burgeoning field of network physiology, dedicated to unraveling these questions, stands to reap substantial benefits through the adoption of analytical techniques such as multiscale PDF analysis. Furthermore, the field could greatly enhance its insights by refining this method and extending its scope to detect non-Gaussian patterns. The analysis of these non-Gaussian patterns should not be confined to individual signals but should encompass the intricate web of interactions across the various subsystems of the body.

ACKNOWLEDGMENTS

[1] K. M. Newell and K. Jordan, Task constraints and movement organization: A common language, in *Ecological Task Analysis and Movement*, edited by W. E. Davis and G. D. Broadhead (Human Kinetics, Champaign, IL, 2007), pp. 5–23.

[2] G. E. Riccio and T. A. Stoffregen, Affordances as constraints on the control of stance, Hum. Mov. Sci. **7**, 265 (1988).

[3] S. Slobounov and K. Newell, Postural dynamics as a function of skill level and task constraints, Gait Posture **2**, 85 (1994).

[4] T. E. Angelini, E. Hannezo, X. Trepat, M. Marquez, J. J. Fredberg, and D. A. Weitz, Glass-like dynamics of collective cell migration, Proc. Natl. Acad. Sci. USA **108**, 4714 (2011).

[5] P. Dieterich, R. Klages, R. Preuss, and A. Schwab, Anomalous dynamics of cell migration, Proc. Natl. Acad. Sci. USA **105**, 459 (2008).

[6] P. Dieterich, O. Lindemann, M. L. Moskopp, S. Tauzin, A. Huttenlocher, R. Klages, A. Chechkin, and A. Schwab, Anomalous diffusion and asymmetric tempering memory in

neutrophil chemotaxis, PLoS Comput. Biol. **18**, e1010089 (2022).

[7] I. Golding and E. C. Cox, Physical nature of bacterial cytoplasm, Phys. Rev. Lett. **96**, 098102 (2006).

[8] S. Hapca, J. W. Crawford, and I. M. Young, Anomalous diffusion of heterogeneous populations characterized by normal diffusion at the individual level, J. R. Soc. Interface **6**, 111 (2009).

[9] A. Lagarde, N. Dagès, T. Nemoto, V. Démery, D. Bartolo, and T. Gibaud, Colloidal transport in bacteria suspensions: From bacteria collision to anomalous and enhanced diffusion, Soft Matter **16**, 7503 (2020).

[10] S. Mukherjee, R. K. Singh, M. James, and S. S. Ray, Anomalous diffusion and Lévy walks distinguish active from inertial turbulence, Phys. Rev. Lett. **127**, 118001 (2021).

[11] S. Benhamou, How many animals really do the Lévy walk? Ecology **88**, 1962 (2007).

[12] A. James, M. J. Plank, and A. M. Edwards, Assessing Lévy walks as models of animal foraging, J. R. Soc. Interface **8**, 1233 (2011).

[13] A. M. Reynolds and C. J. Rhodes, The Lévy flight paradigm: Random search patterns and mechanisms, Ecology **90**, 877 (2009).

[14] C. T. Brown, L. S. Liebovitch, and R. Glendon, Lévy flights in Dobe Ju/'hoansi foraging patterns, Hum. Ecol. **35**, 129 (2007).

[15] D. A. Raichlen, B. M. Wood, A. D. Gordon, A. Z. Mabulla, F. W. Marlowe, and H. Pontzer, Evidence of Lévy walk foraging patterns in human hunter-gatherers, Proc. Natl. Acad. Sci. USA **111**, 728 (2014).

[16] A. G. Cherstvy, D. Vinod, E. Aghion, I. M. Sokolov, and R. Metzler, Scaled geometric Brownian motion features sub- or superexponential ensemble-averaged, but linear time-averaged mean-squared displacements, Phys. Rev. E **103**, 062127 (2021).

[17] V. Plerou, P. Gopikrishnan, L. A. Nunes Amaral, X. Gabaix, and H. E. Stanley, Economic fluctuations and anomalous diffusion, Phys. Rev. E **62**, R3023(R) (2000).

[18] A. Vázquez, J. G. Oliveira, Z. Dezsö, K.-I. Goh, I. Kondor, and A.-L. Barabási, Modeling bursts and heavy tails in human dynamics, Phys. Rev. E **73**, 036127 (2006).

[19] A.-L. Barábasi, The origin of bursts and heavy tails in human dynamics, Nature (London) **435**, 207 (2005).

[20] A. Gelman, Bursts: The hidden pattern behind everything we do, Phys. Today **63**(5), 46 (2010).

[21] J. L. Cabrera and J. G. Milton, On-off intermittency in a human balancing task, Phys. Rev. Lett. **89**, 158702 (2002).

[22] R. D. Malmgren, D. B. Stouffer, A. E. Motter, and L. A. Amaral, A Poissonian explanation for heavy tails in e-mail communication, Proc. Natl. Acad. Sci. USA **105**, 18153 (2008).

[23] T. Nakamura, K. Kiyono, K. Yoshiuchi, R. Nakahara, Z. R. Struzik, and Y. Yamamoto, Universal scaling law in human behavioral organization, Phys. Rev. Lett. **99**, 138103 (2007).

[24] F. A. Oliveira, R. M. Ferreira, L. C. Lapas, and M. H. Vainstein, Anomalous diffusion: A basic mechanism for the evolution of inhomogeneous systems, Front. Phys. **7**, 18 (2019).

[25] I. M. Sokolov and J. Klafter, From diffusion to anomalous diffusion: A century after Einstein's Brownian motion, Chaos **15**, 026103 (2005).

[26] S. F. Timashev, Y. S. Polyakov, P. I. Misurkin, and S. G. Lakeev, Anomalous diffusion as a stochastic component in the dynamics of complex processes, Phys. Rev. E **81**, 041128 (2010).

[27] L. A. Lipsitz and A. L. Goldberger, Loss of 'complexity' and aging: Potential applications of fractals and chaos theory to senescence, JAMA **267**, 1806 (1992).

[28] D. E. Vaillancourt and K. M. Newell, Changing complexity in human behavior and physiology through aging and disease, Neurobiol. Aging **23**, 1 (2002).

[29] J.-P. Eckmann, Roads to turbulence in dissipative dynamical systems, Rev. Mod. Phys. **53**, 643 (1981).

[30] Y. Pomeau and P. Manneville DPh. G. PSRM, Intermittent transition to turbulence in dissipative dynamical systems, Commun. Math. Phys. **74**, 189 (1980).

[31] J. F. Heagy, N. Platt, and S. M. Hammel, Characterization of on-off intermittency, Phys. Rev. E **49**, 1140 (1994).

[32] N. Platt, E. A. Spiegel, and C. Tresser, On-off intermittency: A mechanism for bursting, Phys. Rev. Lett. **70**, 279 (1993).

[33] K. Kiyono, Z. R. Struzik, N. Aoyagi, S. Sakata, J. Hayano, and Y. Yamamoto, Critical scale invariance in a healthy human heart rate, Phys. Rev. Lett. **93**, 178103 (2004).

[34] K. Kiyono, Z. R. Struzik, N. Aoyagi, and Y. Yamamoto, Multiscale probability density function analysis: Non-Gaussian and scale-invariant fluctuations of healthy human heart rate, IEEE Trans. Biomed. Eng. **53**, 95 (2006).

[35] M. R. Giveans, K. Yoshida, B. Bardy, M. Riley, and T. A. Stoffregen, Postural sway and the amplitude of horizontal eye movements, Ecol. Psychol. **23**, 247 (2011).

[36] S. T. Rodrigues, P. F. Polastri, J. C. Carvalho, J. A. Barela, R. Moraes, and F. A. Barbieri, Saccadic and smooth pursuit eye movements attenuate postural sway similarly, Neurosci. Lett. **584**, 292 (2015).

[37] B. Mantel, T. A. Stoffregen, A. Campbell, and B. G. Bardy, Exploratory movement generates higher-order information that is sufficient for accurate perception of scaled egocentric distance, PLoS One **10**, e0120025 (2015).

[38] L. S. Mark, J. A. Balliett, K. D. Craver, S. D. Douglas, and T. Fox, What an actor must do in order to perceive the affordance for sitting, Ecol. Psychol. **2**, 325 (1990).

[39] Y. Yu, B. G. Bardy, and T. A. Stoffregen, Influences of head and torso movement before and during affordance perception, J. Motor Behav. **43**, 45 (2010).

[40] M. Kawato, Internal models for motor control and trajectory planning, Curr. Opin. Neurobiol. **9**, 718 (1999).

[41] R. Shadmehr, M. A. Smith, and J. W. Krakauer, Error correction, sensory prediction, and adaptation in motor control, Annu. Rev. Neurosci. **33**, 89 (2010).

[42] E. Todorov and M. I. Jordan, Optimal feedback control as a theory of motor coordination, Nat. Neurosci. **5**, 1226 (2002).

[43] E. Todorov, Optimality principles in sensorimotor control, Nat. Neurosci. **7**, 907 (2004).

[44] D. M. Wolpert, Z. Ghahramani, and M. I. Jordan, An internal model for sensorimotor integration, Science **269**, 1880 (1995).

[45] D. M. Wolpert and M. Kawato, Multiple paired forward and inverse models for motor control, Neural Networks **11**, 1317 (1998).

[46] D. M. Wolpert and Z. Ghahramani, Computational principles of movement neuroscience, Nat. Neurosci. **3**, 1212 (2000).

[47] H. H. Pattee and J. Raczaszek-Leonardi, *Laws, Language and Life: Howard Pattee's Classic Papers on the Physics of Symbols with Contemporary Commentary*, Biosemiotics Vol. 7 (Springer, New York, 2012).

[48] E. A. Ihlen and B. Vereijken, Interaction-dominant dynamics in human cognition: Beyond $1/f^\alpha$ fluctuation, J. Exp. Psychol.: Gen. **139**, 436 (2010).

[49] B. Mandelbrot, Intermittent turbulence and fractal dimension: Kurtosis and the spectral exponent 5/3+B, in *Turbulence and Navier Stokes Equations*, edited by C. Foias (Springer, Berlin, 1976), pp. 121–145.

[50] B. G. Tabachnick, L. S. Fidell, and J. B. Ullman, *Using Multivariate Statistics*, 5th ed. (Pearson, Boston, MA, 2007).

[51] J. G. Holden, G. C. Van Orden, and M. T. Turvey, Dispersion of response times reveals cognitive dynamics, Psychol. Rev. **116**, 318 (2009).

[52] D. G. Stephen and D. Mirman, Interactions dominate the dynamics of visual cognition, Cognition **115**, 154 (2010).

[53] J. S. Kelso, *Dynamic Patterns: The Self-Organization of Brain and Behavior* (MIT Press, Cambridge, MA, 1995).

[54] J. S. Kelso, D. A. Engstrom, and D. Engstrom, *The Complementary Nature* (MIT Press, Cambridge, MA, 2006).

[55] E. A. Codling, M. J. Plank, and S. Benhamou, Random walk models in biology, J. R. Soc. Interface **5**, 813 (2008).

[56] M. A. Lomholt, K. Tal, R. Metzler, and K. Joseph, Lévy strategies in intermittent search processes are advantageous, Proc. Natl. Acad. Sci. USA **105**, 11055 (2008).

[57] A. Clauset, C. R. Shalizi, and M. E. Newman, Power-law distributions in empirical data, SIAM Rev. **51**, 661 (2009).

[58] A. M. Edwards, R. A. Phillips, N. W. Watkins, M. P. Freeman, E. J. Murphy, V. Afanasyev, S. V. Buldyrev, M. G. da Luz, E. P. Raposo, H. E. Stanley, G. M. Viswanathan, Revisiting Lévy flight search patterns of wandering albatrosses, bumblebees and deer, Nature (London) **449**, 1044 (2007).

[59] L. S. Liebovitch and W. Yang, Transition from persistent to antipersistent correlation in biological systems, Phys. Rev. E **56**, 4557 (1997).

[60] M. F. Shlesinger, B. J. West, and J. Klafter, Lévy dynamics of enhanced diffusion: Application to turbulence, Phys. Rev. Lett. **58**, 1100 (1987).

[61] B. Castaing, Y. Gagne, and E. Hopfinger, Velocity probability density functions of high Reynolds number turbulence, Phys. D (Amsterdam) **46**, 177 (1990).

[62] R. H. Kraichnan, Models of intermittency in hydrodynamic turbulence, Phys. Rev. Lett. **65**, 575 (1990).

[63] K. Kiyono, Z. R. Struzik, N. Aoyagi, F. Togo, and Y. Yamamoto, Phase transition in a healthy human heart rate, Phys. Rev. Lett. **95**, 058101 (2005).

[64] K. Kiyono, J. Hayano, E. Watanabe, Z. R. Struzik, and Y. Yamamoto, Non-Gaussian heart rate as an independent predictor of mortality in patients with chronic heart failure, Heart Rhythm **5**, 261 (2008).

[65] B. J. West and M. Turalska, Hypothetical control of heart rate variability, Front. Physiol. **10**, 1078 (2019).

[66] M. Fukuda, Y. Ogiyama, R. Sato, T. Miura, H. Fukuta, M. Mizuno, K. Kiyono, Y. Yamamoto, J. Hayano, and N. Ohte, L/T-type calcium channel blocker reduces non-Gaussianity of heart rate variability in chronic kidney disease patients under preceding treatment with ARB, J. Renin-Angiotensin-Aldosterone Syst. **17**, 147032031664390 (2016).

[67] T. Nakamura, K. Kiyono, H. Wendt, P. Abry, and Y. Yamamoto, Multiscale analysis of intensive longitudinal biomedical signals and its clinical applications, Proc. IEEE **104**, 242 (2016).

[68] L. A. Safonov, Y. Isomura, S. Kang, Z. R. Struzik, T. Fukai, and H. Câteau, Near scale-free dynamics in neural population activity of waking/sleeping rats revealed by multiscale analysis, PLoS One **5**, e12869 (2010).

[69] M. P. Furmanek, M. Mangalam, D. G. Kelty-Stephen, and G. Juras, Postural constraints recruit shorter-timescale processes into the non-Gaussian cascade processes, Neurosci. Lett. **741**, 135508 (2021).

[70] D. G. Kelty-Stephen, M. P. Furmanek, and M. Mangalam, Multifractality distinguishes reactive from proactive cascades in postural control, Chaos, Solitons Fractals **142**, 110471 (2021).

[71] M. Mangalam and D. G. Kelty-Stephen, Hypothetical control of postural sway, J. R. Soc. Interface **18**, 20200951 (2021).

[72] M. Mangalam, I.-C. Lee, K. M. Newell, and D. G. Kelty-Stephen, Visual effort moderates postural cascade dynamics, Neurosci. Lett. **742**, 135511 (2021).

[73] J. Hayano, K. Kiyono, Z. R. Struzik, Y. Yamamoto, E. Watanabe, P. K. Stein, L. L. Watkins, J. A. Blumenthal, and R. M. Carney, Increased non-Gaussianity of heart rate variability predicts cardiac mortality after an acute myocardial infarction, Front. Physiol. **2**, 65 (2011).

[74] K. Kiyono, J. Hayano, S. Kwak, E. Watanabe, and Y. Yamamoto, Non-Gaussianity of low frequency heart rate variability and sympathetic activation: Lack of increases in multiple system atrophy and Parkinson disease, Front. Physiol. **3**, 34 (2012).

[75] K. Kiyono, Log-amplitude statistics of intermittent and non-Gaussian time series, Phys. Rev. E **79**, 031129 (2009).

[76] K. Kiyono and H. Konno, Log-amplitude statistics for Beck-Cohen superstatistics, Phys. Rev. E **87**, 052104 (2013).

[77] A. R. Abate and D. J. Durian, Approach to jamming in an air-fluidized granular bed, Phys. Rev. E **74**, 031308 (2006).

[78] T. Kajiya, T. Narita, V. Schmitt, F. Lequeux, and L. Talini, Slow dynamics and intermittent quakes in soft glassy systems, Soft Matter **9**, 11129 (2013).

[79] F. Giesbrecht and O. Kempthorne, Maximum likelihood estimation in the three-parameter lognormal distribution, J. R. Stat. Soc.: Ser. B (Methodological) **38**, 257 (1976).

[80] I. J. Myung, Tutorial on maximum likelihood estimation, J. Math. Psychol. **47**, 90 (2003).

[81] J.-X. Pan and K.-T. Fang, Maximum likelihood estimation, in *Growth Curve Models and Statistical Diagnostics* (Springer, New York, 2002), pp. 77–158.

[82] K. Kiyono, Establishing a direct connection between detrended fluctuation analysis and Fourier analysis, Phys. Rev. E **92**, 042925 (2015).

[83] K. Kiyono and Y. Tsujimoto, Time and frequency domain characteristics of detrending-operation-based scaling analysis:

Exact DFA and DMA frequency responses, Phys. Rev. E **94**, 012111 (2016).

[84] C.-K. Peng, S. V. Buldyrev, S. Havlin, M. Simons, H. E. Stanley, and A. L. Goldberger, Mosaic organization of DNA nucleotides, Phys. Rev. E **49**, 1685 (1994).

[85] C.-K. Peng, S. Havlin, H. E. Stanley, and A. L. Goldberger, Quantification of scaling exponents and crossover phenomena in nonstationary heartbeat time series, Chaos **5**, 82 (1995).

[86] R. W. Schafer, What is a Savitzky-Golay filter?, IEEE Signal Process. Mag. **28**, 111 (2011).

[87] A. Savitzky and M. J. Golay, Smoothing and differentiation of data by simplified least squares procedures, Anal. Chem. **36**, 1627 (1964).

[88] Y. Tsujimoto, Y. Miki, E. Watanabe, J. Hayano, Y. Yamamoto, T. Nomura, and K. Kiyono, Fast algorithm of long-range cross-correlation analysis using Savitzky-Golay detrending filter and its application to biosignal analysis, in *2017 International Conference on Noise and Fluctuations (ICNF)* (IEEE, Piscataway, NJ, 2017), pp. 1–4.

[89] S. Agarwal, A. Rani, V. Singh, and A. P. Mittal, EEG signal enhancement using cascaded S-Golay filter, Biomed. Signal Process. Control **36**, 194 (2017).

[90] A. Carbone and K. Kiyono, Detrending moving average algorithm: Frequency response and scaling performances, Phys. Rev. E **93**, 063309 (2016).

[91] A. Nakata, M. Kaneko, C. Taki, N. Evans, T. Shigematsu, T. Kimura, and K. Kiyono, Assessment of long-range cross-correlations in cardiorespiratory and cardiovascular interactions, Philos. Trans. R. Soc. A **379**, 20200249 (2021).

[92] J.-F. Muzy, E. Bacry, R. Baile, and P. Poggi, Uncovering latent singularities from multifractal scaling laws in mixed asymptotic regime. Application to turbulence, Europhys. Lett. **82**, 60007 (2008).

[93] D. G. Kelty-Stephen, E. Lane, L. Bloomfield, and M. Mangalam, Multifractal test for nonlinearity of interactions across scales in time series, Behav. Res. Methods **55**, 2249 (2023).

[94] N. Wiener, *Time Series* (MIT Press, Cambridge, MA, 1964).

[95] R. I. Kitney and O. Rompelman, *The Study of Heart-Rate Variability* (Clarendon, Oxford, 1980).

[96] J. S. Matthis, K. S. Muller, K. L. Bonnen, and M. M. Hayhoe, Retinal optic flow during natural locomotion, PLoS Comput. Biol. **18**, e1009575 (2022).

[97] A. S. Mauss and A. Borst, Optic flow-based course control in insects, Curr. Opin. Neurobiol. **60**, 21 (2020).

[98] J. K. O'regan, Solving the "real" mysteries of visual perception: The world as an outside memory, Can. J. Psychol. **46**, 461 (1992).

[99] D. G. Kelty-Stephen, K. Palatinus, E. Saltzman, and J. A. Dixon, A tutorial on multifractality, cascades, and interactivity for empirical time series in ecological science, Ecol. Psychol. **25**, 1 (2013).

[100] D. G. Kelty-Stephen, I. C. Lee, N. S. Carver, K. M. Newell, and M. Mangalam, Multifractal roots of suprapostural dexterity, Hum. Mov. Sci. **76**, 102771 (2021).

[101] B. Manor, M. D. Costa, K. Hu, E. Newton, O. Starobinets, H. G. Kang, C. Peng, V. Novak, and L. A. Lipsitz, Physiological complexity and system adaptability: Evidence from postural control dynamics of older adults, J. Appl. Physiol. **109**, 1786 (2010).

[102] M. Mangalam and D. G. Kelty-Stephen, Multiplicative-cascade dynamics supports whole-body coordination for perception via effortful touch, Hum. Mov. Sci. **70**, 102595 (2020).

[103] M. Mangalam, N. S. Carver, and D. G. Kelty-Stephen, Multifractal signatures of perceptual processing on anatomical sleeves of the human body, J. R. Soc. Interface **17**, 20200328 (2020).

[104] D. A. Dos Santos, C. A. Fukuchi, R. K. Fukuchi, and M. Duarte, A data set with kinematic and ground reaction forces of human balance, PeerJ **5**, e3626 (2017).

[105] C. E. N. de Oliveira, C. R. de Souza, R. de Castro Treza, S. M. Hondo, C. Bernardo, T. K. F. Shida, L. d. S. de Oliveira, T. M. Novaes, D. d. S. F. de Campos, E. Gisoldi, M. de Jesus Carvalho, and D. Boari Coelho, A public data set with ground reaction forces of human balance in individuals with Parkinson's disease, Front. Neurosci. **16**, 865882 (2022).

[106] Y. Asai, Y. Tasaka, K. Nomura, T. Nomura, M. Casadio, and P. Morasso, A model of postural control in quiet standing: Robust compensation of delay-induced instability using intermittent activation of feedback control, PLoS One **4**, e6169 (2009).

[107] A. Bottaro, Y. Yasutake, T. Nomura, M. Casadio, and P. Morasso, Bounded stability of the quiet standing posture: An intermittent control model, Hum. Mov. Sci. **27**, 473 (2008).

[108] R. Dash, V. V. Shah, and H. J. Palanthandalam-Madapusi, Explaining Parkinsonian postural sway variabilities using intermittent control theory, J. Biomech. **105**, 109791 (2020).

[109] T. Cluff, T. Gharib, and R. Balasubramaniam, Attentional influences on the performance of secondary physical tasks during posture control, Exp. Brain Res. **203**, 647 (2010).

[110] J. J. Collins and C. J. De Luca, Open-loop and closed-loop control of posture: A random-walk analysis of center-of-pressure trajectories, Exp. Brain Res. **95**, 308 (1993).

[111] J. Collins and C. De Luca, The effects of visual input on open-loop and closed-loop postural control mechanisms, Exp. Brain Res. **103**, 151 (1995).

[112] T. T. Yeh, J. Boulet, T. Cluff, and R. Balasubramaniam, Contributions of delayed visual feedback and cognitive task load to postural dynamics, Neurosci. Lett. **481**, 173 (2010).

[113] T. T. Yeh, T. Cluff, and R. Balasubramaniam, Visual reliance for balance control in older adults persists when visual information is disrupted by artificial feedback delays, PLoS One **9**, e91554 (2014).

[114] V. M. Zatsiorsky and M. Duarte, Instant equilibrium point and its migration in standing tasks: Rambling and trembling components of the stabilogram, Motor Control **3**, 28 (1999).

[115] V. M. Zatsiorsky and M. Duarte, Rambling and trembling in quiet standing, Motor Control **4**, 185 (2000).

[116] D. A. Winter, Human balance and posture control during standing and walking, Gait Posture **3**, 193 (1995).

[117] D. A. Winter, A. E. Patla, F. Prince, M. Ishac, and K. Gielo-Perczak, Stiffness control of balance in quiet standing, J. Neurophysiol. **80**, 1211 (1998).

[118] D. A. Winter, A. E. Patla, M. Ishac, and W. H. Gage, Motor mechanisms of balance during quiet standing, J. Electromyogr. Kinesiol. **13**, 49 (2003).

[119] A. M. Bacsi and J. G. Colebatch, Evidence for reflex and perceptual vestibular contributions to postural control, Exp. Brain Res. **160**, 22 (2005).

[120] R. Fitzpatrick, D. Burke, and S. C. Gandevia, Loop gain of reflexes controlling human standing measured with the use of postural and vestibular disturbances, J. Neurophysiol. **76**, 3994 (1996).

[121] G. N. Gantchev and D. M. Dimitrova, Anticipatory postural adjustments associated with arm movements during balancing on unstable support surface, Int. J. Psychophysiol. **22**, 117 (1996).

[122] M. Klous, P. Mikulic, and M. L. Latash, Two aspects of feed-forward postural control: Anticipatory postural adjustments and anticipatory synergy adjustments, J. Neurophysiol. **105**, 2275 (2011).

[123] M. Klous, P. Mikulic, and M. L. Latash, Early postural adjustments in preparation to whole-body voluntary sway, J. Electromyogr. Kinesiol. **22**, 110 (2012).

[124] R. J. Peterka, Sensorimotor integration in human postural control, J. Neurophysiol. **88**, 1097 (2002).

[125] R. J. Peterka and P. J. Loughlin, Dynamic regulation of sensorimotor integration in human postural control, J. Neurophysiol. **91**, 410 (2004).

[126] M. Carpenter, C. Murnaghan, and J. Inglis, Shifting the balance: Evidence of an exploratory role for postural sway, Neuroscience **171**, 196 (2010).

[127] C. Murnaghan, B. Horslen, J. Inglis, and M. Carpenter, Exploratory behavior during stance persists with visual feedback, Neuroscience **195**, 54 (2011).

[128] I.-C. Lee, M. M. Pacheco, and K. M. Newell, The precision demands of viewing distance modulate postural coordination and control, Hum. Mov. Sci. **66**, 425 (2019).

[129] S. Gheorghiu and M.-O. Coppens, Heterogeneity explains features of "anomalous" thermodynamics and statistics, Proc. Natl. Acad. Sci. USA **101**, 15852 (2004).

[130] L. A. Nunes. Amaral, P. C. Ivanov, N. Aoyagi, I. Hidaka, S. Tomono, A. L. Goldberger, H. E. Stanley, and Y. Yamamoto, Behavioral-independent features of complex heartbeat dynamics, Phys. Rev. Lett. **86**, 6026 (2001).

[131] A. L. Goldberger, L. A. Amaral, J. M. Hausdorff, P. C. Ivanov, C.-K. Peng, and H. E. Stanley, Fractal dynamics in physiology: Alterations with disease and aging, Proc. Natl. Acad. Sci. USA **99**, 2466 (2002).

[132] A. L. Goldberger, C.-K. Peng, and L. A. Lipsitz, What is physiologic complexity and how does it change with aging and disease? Neurobiol. Aging **23**, 23 (2002).

[133] P. C. Ivanov, L. A. N. Amaral, A. L. Goldberger, S. Havlin, M. G. Rosenblum, Z. R. Struzik, and H. E. Stanley, Multifractality in human heartbeat dynamics, Nature (London) **399**, 461 (1999).

[134] K. M. Saqr, S. Tupin, S. Rashad, T. Endo, K. Niizuma, T. Tominaga, and M. Ohta, Physiologic blood flow is turbulent, Sci. Rep. **10**, 15492 (2020).

[135] R. P. Bartsch, K. K. Liu, A. Bashan, and P. C. Ivanov, Network physiology: How organ systems dynamically interact, PLoS One **10**, e0142143 (2015).

[136] A. Bashan, R. P. Bartsch, J. W. Kantelhardt, S. Havlin, and P. C. Ivanov, Network physiology reveals relations between network topology and physiological function, Nat. Commun. **3**, 702 (2012).

[137] P. C. Ivanov, The new field of network physiology: Building the human physiome, Front. Network Physiol. **1**, 711778 (2021).

[138] J. N. Kerkman, A. Daffertshofer, L. L. Gollo, M. Breakspear, and T. W. Boonstra, Network structure of the human musculoskeletal system shapes neural interactions on multiple time scales, Sci. Adv. **4**, eaat0497 (2018).

[139] A. C. Murphy, S. F. Muldoon, D. Baker, A. Lastowka, B. Bennett, M. Yang, and D. S. Bassett, Structure, function, and control of the human musculoskeletal network, PLoS Biol. **16**, e2002811 (2018).

[140] J. Enciso, H. Mayani, L. Mendoza, and R. Pelayo, Modeling the pro-inflammatory tumor microenvironment in acute lymphoblastic leukemia predicts a breakdown of hematopoietic-mesenchymal communication networks, Front. Physiol. **7**, 349 (2016).

[141] B. Foreman, I. A. Lissak, N. Kamireddi, D. Moberg, and E. S. Rosenthal, Challenges and opportunities in multimodal monitoring and data analytics in traumatic brain injury, Current Neurol. Neurosci. Rep. **21**, 6 (2021).

[142] J. R. Moorman, D. E. Lake, and P. C. Ivanov, Early detection of sepsis—a role for network physiology? Crit. Care Med. **44**, e312 (2016).

[143] S. P. Shashikumar, Q. Li, G. D. Clifford, and S. Nemati, Multiscale network representation of physiological time series for early prediction of sepsis, Physiol. Meas. **38**, 2235 (2017).